agronomy

MDPI

Article

Temporal Emergence and Slope Dependence of RUSLE-Based Erosion Reduction Associated with Cropland Abandonment in Northeast China's Black Soil Region

Wei Song

Key Laboratory of Land Surface Pattern and Simulation, Institute of Geographic Sciences and Natural Resources Research, Chinese Academy of Sciences, Beijing 100101, China; songw@igsnrr.ac.cn; Tel.: +86-10-6488-9450

Abstract

Cropland abandonment is expanding, but the timing and slope dependence of modelled erosion contrasts and residual soil loss remain poorly resolved. The study reconstructed continuous abandonment in Northeast China's black soil region using 30 m annual land cover data (2000–2023) and 30 m RUSLE-based water erosion estimates (2000–2020), with local contemporaneous continuously cultivated controls. By 2020, land with event-time Age >10 represented 48.91% of continuously abandoned cropland. The relative reduction metric was small and uncertain at the cropland-exit event anchor (Age 1; 2.13%), reached 40.56% in the first complete post-exit year (Age 2), and remained at 47–50% during Ages 4–17. The operational stable reduction criterion was met earlier on 0–5° slopes than on steeper land, where early and long-term contrasts were weaker. Across 6040 10 km × 10 km cells with continuous abandonment, model-based residual loss totalled 1.090 × 10^6 t yr^{-1}. Unadjusted 15 km Getis–Ord Gi* hot spots at ≥95% confidence occupied 15.0% of all cells but contained 55.5% of residual loss; two high-loss zones occupied 22.20% of abandonment-containing cells but contained 64.9% of residual loss. Continuous abandonment was associated with lower modelled hillslope water erosion without eliminating absolute pressure. Because regional field validation was unavailable, priorities for recently abandoned moderate-to-steep slopes and high-loss areas remain indicative pending field confirmation.

Keywords: Northeast China black soil region; cropland abandonment; RUSLE-based water erosion; event time; slope dependence; soil and water conservation

Academic Editor: Andrea Baglieri

Received: 28 August 2026
Revised: 18 September 2026
Accepted: 21 September 2026
Published: 24 September 2026

1. Introduction

Population growth, changing diets and climate change are placing agricultural systems under simultaneous pressure to stabilise food supplies and sustain land resources [1,2]. Cropland therefore supports not only food production but also soil retention, ecological stability and the persistence of agricultural landscapes. Declining farm returns, labour migration, population ageing and the withdrawal of marginal land have made cropland abandonment a widespread form of land use transition across agricultural regions [3–6]. By removing recurrent cultivation, abandonment can create space for vegetation recovery and ecosystem reassembly, but it also withdraws productive land and changes management needs. Resolving how soil erosion responds after cultivation ceases is therefore central to reconciling food security, sustainable land use and ecological protection.

Rapid urbanisation, rural outmigration and changing farm operating conditions have continued to reshape cropland use in China, drawing attention to abandonment in hilly and mountainous areas, remote regions and agricultural margins [7–9]. Research has characterised its extent, spatial pattern, drivers and ecological effects, and has revealed pronounced spatiotemporal dynamics of abandonment and recultivation in Northeast China [10]. As the focus has shifted from where abandonment occurs to how ecological processes change afterwards, soil and hydrological responses have become a central concern. Once agricultural disturbance ceases, vegetation establishment, root development and litter accumulation can protect the surface and reduce soil erodibility by improving aggregate stability, pore structure and infiltration [11–13]. This protection is not immediate. Sparse cover, exposed-soil patches and inherited flow pathways can sustain runoff and sediment transport during early abandonment, particularly on steep slopes or under extreme rainfall [14–16]. This study evaluates water erosion modelled with the Revised Universal Soil Loss Equation (RUSLE). The response variable is therefore RUSLE-based hillslope water erosion, which represents rainfall–runoff-driven interrill and rill erosion and does not represent field-measured soil loss or capture gully, wind or freeze–thaw erosion, all of which are relevant in Northeast China's black soil region.

Ecological recovery after abandonment accumulates over time, making time elapsed after cultivation ceases a key dimension of soil erosion change. Long-term plots and restoration chronosequences show that vegetation cover, soil structure and hillslope runoff–erosion processes can change in distinct stages as recovery proceeds [15–17]. Regional studies, however, still commonly identify abandonment from a single date or a few land use snapshots. Even time-series studies that consider abandonment frequency or duration have rarely linked a reconstructed, uninterrupted post-exit trajectory to same-year erosion estimates at annual resolution [3,7,8]. Static or discontinuous time representations cannot distinguish early abandonment, response establishment and long-term maintenance, and may pool intermittent use, repeated abandonment and land abandoned in different years. The direction and size of the post-exit change are not uniform: they depend on the subsequent land cover type and successional trajectory, the amount of residual bare ground and surface cover, terrain, climate and prior management history. Explicitly representing continuous cropland-exit trajectories with event-time Age is therefore necessary to determine when lower modelled erosion relative to cultivated cropland becomes evident and whether this contrast persists.

Duration alone cannot explain regional erosion contrasts because abandonment is spatially selective and the associated erosion response may vary with terrain and local environmental context. Slope, land accessibility and agricultural production conditions can influence where cultivation ceases, so a direct comparison of all abandoned land with all cropland may conflate land use status with environmental setting [4,5,18]. Contemporaneously cultivated reference pixels drawn from the neighbourhood of each abandoned pixel improve spatial comparability. Within this local design, slope may further shift the balance between ecosystem recovery and erosive forcing. Previous work has separately documented associations of recovery time and slope with erosion, but continuous regional evidence remains scarce on whether the timing and long-term magnitude of the erosion contrast vary among slope classes [16–20]. Nor does a relative reduction imply that absolute soil loss has disappeared. Large, steep or recently abandoned areas may still contribute substantial soil loss even when their erosion intensity is lower than that of nearby cultivated land. Management therefore requires more than determining whether abandoned land exhibits lower modelled erosion than nearby continuously cultivated land; it also requires assessment of the magnitude, spatial concentration and priority locations of residual soil loss where this relative contrast is observed [20–24].

The black soil region of Northeast China is both a national grain-production core and an area highly susceptible to soil erosion. Extensive cropland and long, gentle hillslopes form a distinctive sloping agricultural landscape. In this region, wind, freeze–thaw and gully erosion operate alongside water erosion, so any assessment based on a RUSLE-type model must be interpreted within that process domain. Prolonged cultivation, use of sloping cropland and topsoil loss have thinned the plough layer and depleted nutrients and productivity in parts of the region [21,23,25–29], while continuing abandonment has intertwined land use transition, natural recovery and hillslope erosion [10]. Studies have compared erosion between abandoned and cultivated cropland, but they have not systematically resolved how this contrast evolves during uninterrupted abandonment, how its establishment varies among slope classes, or where high soil loss pressure persists despite lower modelled erosion relative to local cultivated controls. The study addressed these gaps by comparing abandoned pixels with contemporaneously cultivated local controls, introducing event-time Age into the regional analysis, and linking the temporal response to slope differentiation and residual soil loss. Specifically, the study (1) retrospectively reconstructed cropland-exit event-anchor years and event-time Age from annual land cover trajectories for 2000–2023 in order to characterise spatiotemporal change and event-time Age structure; (2) quantified erosion differences across event-time Age against contemporaneously cultivated local references, identified when a stable relative erosion contrast became evident, and assessed how its timing and long-term magnitude varied among slope classes; and (3) assessed residual soil loss pressure and spatial clustering at the end of the study period to delineate priorities for differentiated soil and water conservation. Rather than claiming that previous work lacks time-series analysis, this study contributes an event-time reconstruction of persistent cropland exit, an annual linkage between that event time and modelled erosion, and a comparison against contemporaneously cultivated local controls.

2. Materials and Methods

2.1. Study Area

The black soil region lies in Northeast China, extending from the Greater Khingan Mountains in the north to southern Liaoning Province, and from the eastern mountain margin of Inner Mongolia in the west to the Ussuri and Tumen rivers in the east. It encompasses Heilongjiang, Jilin and Liaoning provinces and eastern Inner Mongolia (Figure 1a). Low and middle mountains border the region to the east, west and north, enclosing plains and gently rolling hills. Plains, terraces, hills and mountains coexist within a well-developed drainage network, producing clear elevation and slope gradients from the low interior plains to the surrounding mountains (Figure 1b–d). The temperate monsoon climate has marked seasonal and spatial hydrothermal gradients. Precipitation generally increases from west to east (Figure 1f), influencing vegetation recovery, runoff and erosion.

The analysis extent was defined using the boundary dataset of the black soil region and the typical black soil region of Northeast China [30], in which the typical black soil region was delineated primarily from the concentrated distribution of black soils and chernozems. The original typical black soil region covers approximately 333,022.82 km^2. After applying a common valid-data mask and the analysis constraints described in Section 2.2, the final analysis extent represented approximately 95.16% of that original area. The boundary is a vector delineation rather than a surveyed perimeter; results near the boundary should therefore be regarded as approximate, and pixels outside it were excluded from all analyses.

https://doi.org/10.3390/agronomy16191881

The region is characterised by dark, humus-rich topsoil and high inherent fertility, and is one of China's principal commodity-grain production bases. Cropland, forest and grassland dominate land use. Cropland is concentrated on the interior plains and gentle hills and extends locally onto piedmont terraces and hillslopes, whereas forest and grassland occur mainly in the peripheral mountains and western areas (Figure 1e). Since large-scale reclamation, intensive cultivation combined with water, wind and freeze–thaw erosion has thinned the black soil layer, depleted organic matter and impaired soil function on some sloping cropland. These pronounced climatic, geomorphic and land use gradients make the region well suited to examine the establishment of post-abandonment erosion responses, their slope dependence and differentiated management of residual soil loss pressure.

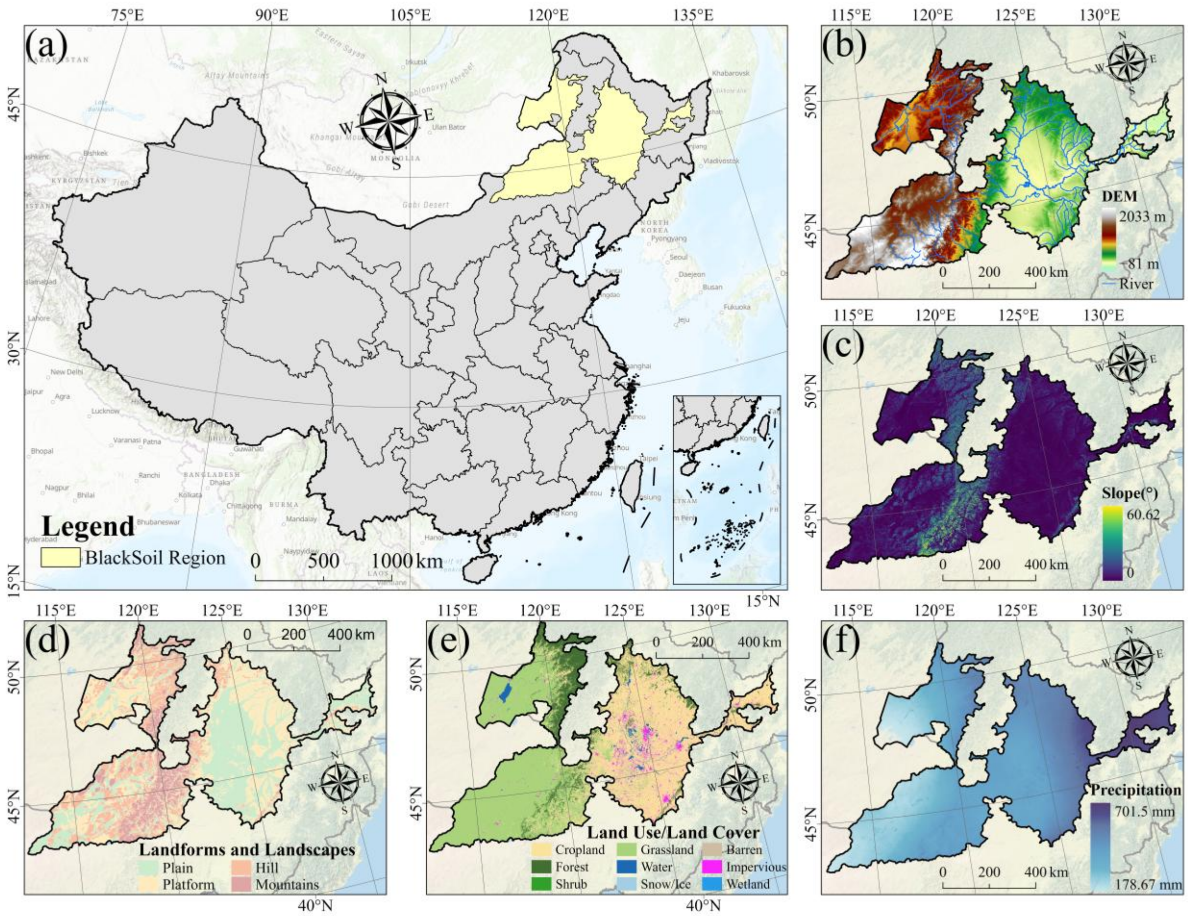

Figure 1. Overview of the study area. (**a**) Geographical location; (**b**) digital elevation model (DEM); (**c**) slope; (**d**) landform types; (**e**) land use/land cover; and (**f**) spatial distribution of precipitation.

2.2. Data Sources

The study integrated annual land cover and RUSLE-based hillslope water erosion data with a digital elevation model (DEM), derived slope and the boundary of the Northeast China black soil region (Table 1). Land cover data were obtained from the 30 m China Land Cover Dataset (CLCD) for 2000–2023 and were used to retrospectively identify cropland-exit events, construct event-time Age, and select local continuously cultivated controls [30]. The CLCD was produced from Landsat imagery using random forest classification with spatiotemporal consistency post-processing. Based on 5463 independent manually interpreted samples, its annual overall accuracy ranges from 76.45% to 82.51%

(mean 79.30 ± 1.99%); the mean F1 is 85.49 ± 1.30% for forest and above 72% for grassland. For cropland, which is the class most critical to this study, producer's accuracy, user's accuracy and F1 are 73.66%, 77.73% and 75.64% against the Geo-Wiki reference and 64.52%, 78.43% and 70.80% against the GLCVSS reference. The original nine CLCD classes were recoded to study-specific values 0–5. Cropland was coded as 1, and forest, grassland and unused land as 2, 4 and 5, respectively; the latter three were treated as valid post-abandonment land cover states. These accuracy levels support long-term regional analysis but do not make pixel-level transitions error-free. In particular, confusion between cropland and grassland can advance or delay the assigned event-anchor year, and CLCD uncertainty propagates through two partly shared pathways because CLCD contributes both to cropland-exit detection and to the parameterisation of the CSWED C and P factors; the two error components are therefore not independent. The merged built-up-land and water class and other filtered classes were excluded from abandonment identification. Land cover-based persistent cropland exit therefore cannot be equated with socioeconomic abandonment: forest, grassland and unused-land transitions may also reflect ecological restoration programmes, natural succession, long-term fallow or classification error. Soil erosion was obtained from version 3 of the 30 m annual soil erosion dataset for China (CSWED; Yan et al. [31]), which provides layers for 2000–2022. This Google Earth Engine product applied the Revised Universal Soil Loss Equation (RUSLE) to rainfall erosivity (R), soil erodibility (K), slope length and steepness (LS), cover management (C) and support practice (P) factors. The soil erosion product estimated annual hillslope water erosion using RUSLE ($A = R \times K \times LS \times C \times P$). Its C factor combined CLCD land cover classes with Landsat-derived NDVI and fractional vegetation cover, while the P factor incorporated land cover and slope. Thus, abandonment identification and modelled erosion were partly coupled through shared land cover information. However, the erosion estimates also depended on rainfall, soil, topography and annual vegetation conditions. The study therefore interprets the results as RUSLE-based erosion responses associated with continuous cropland abandonment, rather than independent field measurements of soil loss. Erosion response analysis used the 2000–2020 layers, with soil erosion intensity standardised to t ha^{-1} yr^{-1} [31]. Although CSWED extends to 2022, event identification requires a three-year posterior confirmation window; the 2020 event anchor is confirmed by land cover observations for 2021–2023, so a 2020 anchor is the latest that can be confirmed. Restricting the erosion analysis to 2000–2020 is therefore set by the need for complete retrospective event confirmation, not by truncation of the erosion product. The source CSWED product was evaluated at the national scale against provincial water erosion areas reported in the China Soil and Water Conservation Bulletins for 2018–2022, yielding a five-year mean absolute error of 9.48%, and against observations from 446 runoff plots [31]. These product-level evaluations support the general reliability of the source dataset, but they are national-scale assessments and do not constitute independent validation of modelled erosion on abandoned cropland in Northeast China's black soil region. Because no field plots or sediment records from the study region were available, the modelled erosion responses were not independently validated in this study. RUSLE represents rainfall–runoff-driven interrill and rill erosion; erosion estimates reported here therefore refer specifically to modelled hillslope water erosion and exclude wind, freeze–thaw and gully erosion. Elevation was obtained from Copernicus DEM GLO-30, from which slope was derived. All spatial layers were reprojected to an Albers equal-area conic projection and aligned to a common 30 m analysis grid. Categorical data were resampled by nearest neighbour and continuous data by bilinear interpolation. Pixel area was calculated from the projection geometry rather than assumed to equal 900 m^2, so that area-weighted summaries remain valid where grid cells are clipped by the regional boundary. Pixels outside

https://doi.org/10.3390/agronomy16191881

the study region were set to NoData, and all subsequent analyses were restricted to its boundary.

Table 1. Spatial datasets and their uses.

Data Type	Data Source	Temporal Coverage	Spatial Resolution	Variable (Unit)	Primary Use
Land cover data (CLCD)	Yang and Huang (2026) [30]	2000–2023	30 m	Original 9 CLCD classes; study-specific analysis codes 0–5	Retrospective identification of cropland-exit events, construction of event-time Age, and selection of local continuously cultivated controls.
RUSLE-based hillslope water erosion data	Yan et al. (2025) [32]	2000–2020	30 m	Modelled hillslope water erosion intensity (t ha^{-1} yr^{-1})	Analysis of modelled hillslope water erosion intensity, relative erosion contrasts and residual modelled soil loss pressure
Digital elevation model (DEM)	European Space Agency (ESA)/European Union, Copernicus DEM GLO-30	2020	30 m	Elevation (m)	Terrain characterisation and slope derivation
Slope	Derived from Copernicus DEM GLO-30	2020	30 m	Slope (°)	Slope-by-Age-stratified analysis
Black soil region boundary	Liu et al. (2021) [33]	Static	Vector polygon	Analysis extent	Definition and clipping of the study region

2.3. Analytical Framework

The analytical framework linked cropland abandonment identification, reconstruction of event-time Age, local-control comparisons, slope differentiation, residual soil loss and differentiated management (Figure 2). Annual 30 m land cover sequences for 2000–2023 were used to identify cropland-exit events and subsequent land cover states. A three-year posterior continuity rule was then used to retrospectively confirm each pixel's first continuous post-exit episode and assign its event-anchor year and event-time Age. Each abandoned pixel was compared with contemporaneous cropland that remained cultivated in its neighbourhood. The comparison yielded the erosion intensity difference (ΔE) and the relative erosion contrast (RC), which were used to identify establishment and maintenance of the response across event-time Age.

The study crossed four slope classes (0–5°, 5–15°, 15–25° and >25°) with four event-time Age groups (Ages 1–3, 4–6, 7–10 and >10) to assess topographic modification of the event-time–erosion relationship. For cropland that remained continuously abandoned in 2020, residual soil loss, residual soil loss density and the long-term reduction context were summarised in 10 km × 10 km grids, and Getis–Ord Gi* analysis identified spatial clusters of high residual soil loss. Continuously abandoned area, residual soil loss pressure, long-term reduction context, the proportion of recently abandoned land on steep slopes and the proportion of long-term abandonment were then combined in a sequential rule set to delineate differentiated management zones. The framework thus progressed from abandonment detection and response estimation to slope differentiation and spatial management of residual soil loss.

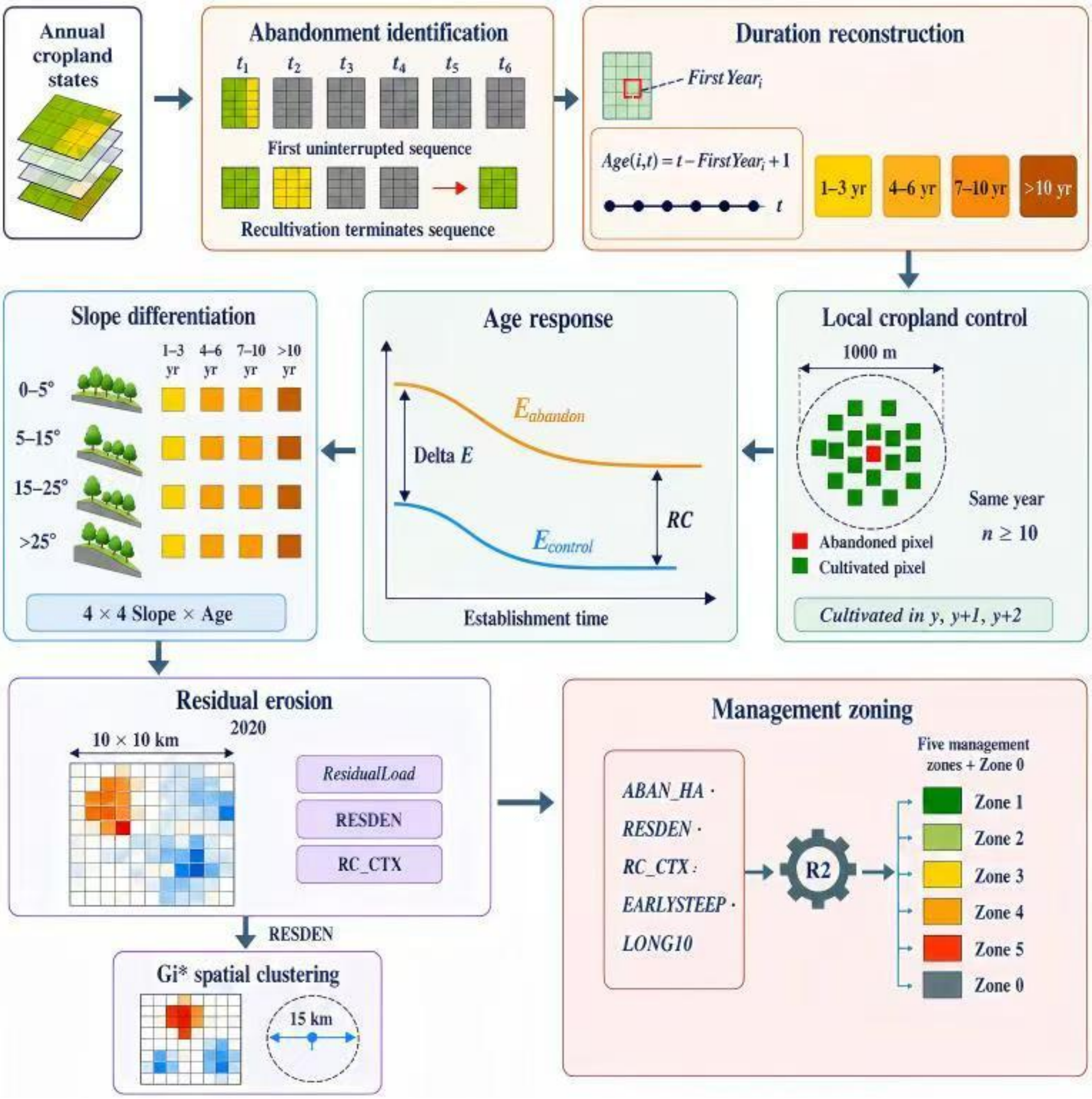

Figure 2. Research framework. First Year in the schematic denotes the retrospectively confirmed cropland-exit event-anchor year Y, not the first post-exit year. Age = t − Y + 1; Age 1 is the last complete year classified as cropland, and Age 2 is the first complete post-exit year. The schematic labels 1–3, 4–6, 7–10 and >10 yr denote event-time Age groups, not elapsed years after cultivation ceased.

2.4. Retrospective Identification of Cropland-Exit Events and Construction of Event-Time Age

Cropland-exit events were identified retrospectively from the annual CLCD sequence. A pixel was assigned an event-anchor year Y when it was classified as cropland in year Y and as forest, grassland or unused land in each of the following three years (Y + 1, Y + 2 and Y + 3). Built-up land, water and other filtered land cover classes were excluded. The three-year posterior window reduced false identification caused by temporary fallow, short-term idling and single-year classification noise. Retrospective confirmation did not shift the event time to Y + 3; year Y remained the event anchor and represented the last complete year in which the pixel was classified as cropland. This three-year persistence requirement is an operational event definition applied to the temporally filtered CLCD sequence; it is distinct from the 3 × 3 × 3 spatiotemporal filtering implemented within the

CLCD product itself, and it cannot fully separate temporary fallow, policy-driven cropland retirement or classification error from socioeconomic abandonment.

For pixel i, the retrospectively confirmed cropland-exit event-anchor year was denoted as $FirstYear_i$. Event-time Age in observation year t was calculated as:

$$Age(i,t) = t - FirstYeari + 1 \tag{1}$$

Accordingly, Age 1 denotes the event-anchor year Y, which is the last complete year in which the pixel was classified as cropland, rather than the first year after abandonment. Age 2 corresponds to Y + 1 and represents the first complete post-exit year. Although an event was confirmed only after observing land cover states through Y + 3, this retrospective confirmation did not shift the assigned event time.

A 2019 event anchor was confirmed using land cover observations for 2020–2022, whereas a 2020 event anchor was confirmed using observations for 2021–2023. The additional land cover observations were used only for retrospective event confirmation; the RUSLE-based erosion response analysis remained restricted to outcomes through 2020.

2.5. Local Cropland Controls and Quantification of Erosion Differences

Each continuously abandoned pixel was compared with spatially proximate cropland in the same observation year. Candidate controls were searched within 1000 m and had to remain cropland in year y and in y + 1 and y + 2, have a valid modelled hillslope water erosion value in year y, and have FirstAbandonYear recorded as NoData or later than y + 2. An abandoned source was eligible only when at least 10 such controls were available. The threshold defined local support; when more than 10 candidates were present, all eligible candidates were retained rather than randomly subsampling 10. Within each 20 km processing core, each strict control was assigned once to the nearest eligible abandoned source within the search radius and was not reused for another source. For each year–Age unit, $E_{control}$ was the arithmetic mean of the assigned controls; pooled $E_{control}$ was weighted by the number of assigned controls, whereas E_{abandon} was aggregated over eligible abandoned pixels using valid comparison area or pixel count. Slope-by-Age analyses additionally required controls and abandoned pixels to belong to the same slope class. This design aligned the comparison by year, neighbourhood, continued cultivation and, where relevant, slope class, but it did not explicitly match soil properties, accessibility, management history or other unobserved factors. The design should therefore be understood as an observational local-reference design rather than causal identification in the sense of a randomised experiment. Because only the published CSWED erosion product was used and consistent annual rasters for the individual R, K, LS, C and P factors are not distributed with it, factor-level perturbation experiments could not be reproduced for every year; this limitation is addressed further in the Discussion.

For each abandoned pixel, we calculated modelled hillslope water erosion intensity E_{abandon} and the corresponding intensity of its local continuously cultivated controls $E_{control}$. The erosion intensity difference ΔE and the relative erosion contrast RC were then defined as:

$$\Delta E = E_{abandon} - E_{control} \tag{2}$$

$$RR = (E_{control} - E_{abandon}) \Big/ E_{control} \times 100\% \tag{3}$$

In Equations (2) and (3), $\Delta E < 0$ indicates lower modelled hillslope water erosion intensity on abandoned land than on local continuously cultivated cropland, and $RC > 0$

indicates a relative erosion reduction advantage. Both metrics describe statistical contrasts with local continuously cultivated cropland; they do not estimate causal treatment effects.

A pre-event balance diagnostic was anchored to the cropland-exit event year f, with t − 2 = f − 2 and t − 1 = f − 1. The same treatment and assigned-control samples were required to be cropland and to have valid erosion values at both pre-event times. This yielded 19 event cohorts (2002–2020). The study evaluated treatment–control differences and standardised mean differences (SMDs) at t − 2 and t − 1, together with the difference in their two-period changes. These diagnostics assess whether future-abandoned and local cultivated pixels had broadly comparable pre-event modelled erosion; they do not establish random assignment or a causal parallel-trends condition.

2.6. Event-Time Response and Identification of a Stable Relative Erosion Contrast

Using local continuously cultivated controls, the study characterised how the statistical contrast in modelled hillslope water erosion varied with event-time Age. At each Age, we summarised $E_{\mathrm{aban}don}$, $E_{control}$, ΔE and RC. Because valid-pixel counts and observation-year composition differed among Ages, we used two complementary summaries. Area-weighted aggregation (AWS) pooled RC results using valid-pixel counts. Observation-year standardisation gave equal weight to each $Year-Age$ unit and reported the mean, median, standard deviation and proportion of positive RC values. The study also summarised the annual estimates in four event-time groups: Ages 1–3, 4–6, 7–10 and >10. The operational stable reduction establishment timing was assigned only when an Age contained at least three independent observation years, $RC>0$ and $\Delta E<0$, at least 67% of $Year-Age$ units had $RC>0$, and the conditions were met for three consecutive Ages. This operational criterion identifies statistical establishment of the response and is not interpreted as a universal ecological threshold.

The requirement of at least three observation years was used to reduce the influence of single-year rainfall anomalies and data noise. The 67% threshold represents a two-thirds directional agreement among valid $Year-Age$ units, which is stricter than a simple majority but does not require all years to show the same response. The study used three consecutive Ages as the baseline persistence window because this length matches the abandonment identification rule. A pixel was classified as continuously abandoned only when the land cover transition persisted for at least three years. Accordingly, the erosion reduction signal was considered stable only when it maintained the same direction across three consecutive Ages. A two-Age window may be more affected by short-term variation between adjacent years, whereas a four-Age window may delay the identification of early responses.

This criterion identifies an operationally defined timing of sustained relative contrast. It is a descriptive statistical rule for the present data and is not interpreted as a universal ecological threshold. The study tested its sensitivity in a 3 × 3 analysis that retained the three core conditions above, varied the positive-RC proportion threshold (60%, 67% and 75%), and required 2, 3 or 4 consecutive qualifying Ages.

Uncertainty in RC and ΔE was assessed using two complementary 5000-replicate cluster bootstraps with 95% percentile confidence intervals. The observation-year bootstrap resampled the 21 observation years with replacement and retained all Age units within each selected year. The 20 km spatial-block bootstrap resampled 1666 spatial cores with replacement and retained all years and Ages within each selected core. The two intervals were reported separately: the first characterises uncertainty associated with year and cohort composition, and the second characterises spatial clustering. The study did not use ordinary pixel-level t tests as the main inferential basis because 30 m observations are spatially and temporally dependent. The spatial-block implementation recomputed

$E_{abandon}$, $E_{control}$, ΔE and RC from block × year × Age sufficient statistics; full-sample estimates reproduced the formal pooled and AWS results to floating-point precision. Because the same abandoned pixel could contribute observations to multiple Age classes across observation years, the spatial-block bootstrap retained all years and Ages within each selected block and thereby preserved repeated spatial contributions; the observation-year bootstrap separately retained all Age units within each selected year.

The study repeated the local-control comparison using search radii of 500, 1000 and 1500 m while retaining the Age definition, continuous-cropland control rule, FirstAbandonYear constraint, minimum support of 10 controls, nearest-source unique assignment, and RC and ΔE estimators. The study reports both the Age response trajectories and valid-comparison coverage because exclusion caused by insufficient local controls need not be spatially random.

To test whether the pooled event-time trajectory concealed differences among post-exit land cover pathways, the analysis was repeated with the Age 2 land cover class defining a fixed pathway label that was retained for all later Ages. Three pathways were distinguished: cropland → forest, cropland → grassland, and cropland → unused/barren. All other elements of the procedure were unchanged, including the 1000 m local search radius, the requirement of at least 10 continuously cultivated controls, the persistence requirements for controls, the FirstAbandonYear restriction and the area-weighted calculation of RC and ΔE. Recombining the pathways reproduced the overall Age 1–21 estimates to within 5.15×10^{-7} percentage points for RC and 8.63×10^{-9} for ΔE, confirming that stratification did not alter the matching or aggregation rules.

2.7. Slope-Stratified Event-Time Response

Slope strata were introduced to assess whether the timing and relative magnitude of the erosion contrast varied with terrain. Four classes were used—0–5°, 5–15°, 15–25° and >25°. The 15° boundary was retained as a geomorphologically meaningful break because it separates gently sloping cropland, where cultivation and contour measures are widely practicable, from steeper sloping cropland that is preferentially targeted by conservation and retirement programmes in the black soil region. Each abandoned pixel was compared only with local continuously cultivated cropland in the same slope class. In addition to being within 1000 m, remaining cultivated during the observation year and two subsequent years, having valid erosion values and providing at least 10 controls, candidate pixels had to share the abandoned pixel's slope class. For each Age, we then calculated $E_{abandon}$, $E_{control}$, ΔE and RC, and crossed the four Age groups (Ages 1–3, 4–6, 7–10 and >10) with the four slope classes to form 16 Slope × Age combinations. A stable positive relative contrast within each slope class was identified using the criteria in Section 3.4, allowing comparison of its establishment time and long-term magnitude among slope classes. Slope-class sensitivity was additionally evaluated using seven finer classes (0–5°, 5–10°, 10–15°, 15–20°, 20–25°, 25–30° and ≥30°), with treatment and assigned controls required to belong to the same fine class. All other aspects of the procedure were unchanged. Re-aggregating the continuous slope raster into the four original classes reproduced the baseline classification for all 616,138,984 comparable pixels, with no mismatched pixels.

2.8. Residual Soil Loss and Spatial Clustering

To represent the soil loss pressure that persisted at the end of the study period, we used 2020 as a status snapshot and partitioned the black soil region into a regular 10 km × 10 km grid, clipping edge cells to the regional boundary. Let Ω_j denote the set of pixels in grid cell j that remained in their first continuous abandonment episode in 2020. Residual annual soil loss for that cell ($ResidualSoilLoss_j$) was calculated as:

$$ResidualSoilLoss_j = \sum_{i \in \Omega_j} E_i A_i \tag{4}$$

where E_i is the 2020 modelled hillslope water erosion intensity of the continuously abandoned pixel i (t ha^{-1} yr^{-1}), and A_i is its actual area (ha). $ResidualSoilLoss_j$ is the annual residual soil loss from continuously abandoned cropland within the grid cell (t yr^{-1}). Because clipping produced edge cells of unequal area, residual soil loss was further standardised by the actual area of the grid cell within the study region, G_j:

$$RSLD_j = \frac{ResidualSoilLoss_j}{G_j} \tag{5}$$

where G_j is expressed in km^2, and $RSLD_j$ is residual soil loss density at the grid scale (t km^{-2} yr^{-1}). This metric integrates modelled hillslope water erosion intensity and the area of continuously abandoned cropland while accounting for variation in edge-cell area. Both $ResidualSoilLoss_j$ and $RSLD_j$ were set to 0 for grid cells containing no continuously abandoned pixels in 2020. ResidualSoilLoss and RESDEN are RUSLE-based estimates of rainfall–runoff-driven hillslope water erosion. They are not direct field measurements and do not include gully, wind or freeze–thaw erosion.

To characterise the long-term erosion response context of each grid cell, we spatially reaggregated the long-term area-weighted AWS_{RC} for the 16 slope-by-Age combinations and derived a grid-scale contextual reduction metric, $RC_{CTX,j}$:

$$RC_{CTX,j} = \frac{\sum_{c=1}^{16} A_{jc} RC_c}{\sum_{c=1}^{16} A_{jc}} \tag{6}$$

where A_{jc} is the continuously abandoned area in grid cell j belonging to slope-by-Age combination c, and RC_c is the long-term AWS_{RC} of combination c relative to local continuously cultivated cropland in the same slope class. $RC_{CTX,j}$ describes only the grid-scale background of long-term erosion reduction; it is neither an observed reduction rate for an individual pixel nor a pixel-level causal effect.

Hereafter, RC_CTX is interpreted only as a class-based expected relative reduction context. It transfers group-level slope × Age estimates to a grid according to its area composition and therefore is neither a direct local observation nor a pixel- or grid-level causal effect.

Using $RSLD$ as the analysis variable, we evaluated local spatial clustering of residual soil loss pressure with Getis–Ord G_j^* hot spot analysis [34,35]. Let x_k denote the value of grid cell k for $RSLD$, and let $w_{jk}(d)$ be the spatial weight under distance threshold d between grid cells j and k. The standardised G_j^* statistic was calculated as:

$$G_j^* = \frac{\sum_{k=1}^{n} w_{jk}(d)x_k - \hat{x}\sum_{k=1}^{n} w_{jk}(d)}{S\sqrt{\dfrac{n\sum_{k=1}^{n} w_{jk}^2(d) - \left[\sum_{k=1}^{n} w_{jk}(d)\right]^2}{n-1}}} \quad (7)$$

$$\hat{x} = \frac{1}{n}\sum_{k=1}^{n} x_k, \quad S = \sqrt{\frac{1}{n}\sum_{k=1}^{n} x_k^2 - \hat{x}^2} \quad (8)$$

where n is the number of grid cells included in the analysis. A 15 km fixed-distance band was used: $W_{jk}(d)=1$ for cells no more than 15 km apart and 0 otherwise. The G_j^* statistic included the focal grid cell. According to the sign and significance of the standardised Z value, cells were classified as hot spots or cold spots significant at the 90%, 95% or 99% confidence level, or as not significant. A hot spot denotes a neighbourhood cluster of high residual soil loss density; it does not imply that every cell within the cluster has the highest $RSLD$.

The 15 km baseline distance had a geometric interpretation for the 10 km grid: it included both orthogonally adjacent cell centres (10 km) and diagonally adjacent cell centres (approximately 14.14 km), thereby approximating a first-order queen neighbourhood. The study evaluated distance band sensitivity by calculating Global Moran's I for RESDEN from 10 to 60 km at 5 km intervals and by repeating Gi* at 10, 15 and 20 km. False discovery rate (FDR) correction was additionally applied to the local Gi* tests to evaluate the influence of multiple testing. The unadjusted 15 km classes were retained as the baseline map, whereas the FDR-adjusted classifications were treated as a robustness analysis. Getis–Ord Gi* was applied only to the spatial clustering of RESDEN and was not used to quantify uncertainty in RC or ΔE.

Spatial-support sensitivity was evaluated using nested 5, 10 and 20 km grids with a common spatial origin. Fixed-distance bands of 7.5, 15 and 30 km, respectively, were used to retain broadly comparable neighbourhood topology. The study verified conservation of total persistent cropland-exit area and ResidualSoilLoss across scales, quantified the share of regional load in high-RESDEN units and significant hot spots, and assessed spatial agreement with area-based Jaccard indices. These analyses evaluated aggregation and boundary sensitivity; they did not propagate classification and RUSLE-factor errors into the regional total.

2.9. Differentiated Management Zoning by Erosion Pressure and Recovery State

To integrate absolute modelled soil loss pressure, class-based recovery context and recovery-stage characteristics, the study developed a rule-based framework for indicative regional management zoning [36,37]. No subjective weights were assigned, and no linearly weighted composite index was constructed. Thresholds were estimated from the 6040 grid cells with persistent cropland exit in 2020. ABAN_HA served only as the inclusion criterion: all cells with ABAN_HA > 0 were assigned to Zones 1–5, whereas the 125 cells with ABAN_HA = 0 formed Zone 0 and were retained only as a spatial background. ABAN_HA percentiles were calculated diagnostically but were not used to screen cells or define a management zone. The percentile cut-offs applied to the other indicators distinguish relative high and low values within the study area and are data-driven operational thresholds, not independently validated ecological or management thresholds.

The 25th and 75th percentiles of RC_CTX were 39.35% and 48.77%, respectively, distinguishing relatively weak from strong long-term reduction contexts. The 75th percentile of RESDEN was 2.674 t km^{-2} yr^{-1}. A cell was classified as having high residual pressure when RESDEN reached this upper-quartile threshold or when the baseline 15 km Gi* analysis identified a hot spot significant at ≥95% confidence (Gi_Bin ≥ 2), thereby combining cell-level pressure with neighbourhood concentration. EARLYSTEEP was the percentage of continuously abandoned area that was both in the Ages 1–3 group and on slopes ≥15°; its 75th percentile across the 6040 positive-area cells was 0.257%. LONG10 was the percentage of continuously abandoned area with Age >10; its 75th percentile was 60%. A fixed decision order ensured mutually exclusive zones.

$$Z_j = \begin{cases} 0, & ABAN\_HA_j = 0; \\ 1, & ABAN\_HA_j \geq 37.8675,\ RESDEN_j \geq 2.674,\ RR_{CTX,j} \leq 39.35; \\ 2, & \text{not assigned to Zone 1, and } ABAN\_HA_j \geq 37.8675,\ EARLYSTEEP_j \geq 1.056; \\ 3, & \text{not assigned to Zone } 1-2\text{, and } ABAN\_HA_j \geq 37.8675,\ RESDEN_j \geq 2.674; \\ 4, & \text{not assigned to Zone } 1-3\text{, and } ABAN\_HA_j \geq 37.8675,\ LONG10_j \geq 60,\ RR_{CTX,j} \geq 48.77; \\ 5, & 0 < ABAN\_HA_j < 37.8675\text{; other grid cells containing contiguous shrubland} \end{cases} \tag{9}$$

Zone 1, the high residual soil loss–weak reduction priority intervention zone, combined high residual pressure with a weak long-term reduction context. Zone 2, the steep-slope early-abandonment transition zone, captured concentrations of recently abandoned land on moderately steep and steep slopes. Zone 3, the high residual soil loss–reduction maintenance zone, had an established long-term reduction context but retained high residual pressure. Zone 4, the long-term abandonment–stable reduction maintenance zone, combined a high proportion of long-term continuous abandonment with a strong reduction context. Zone 5, the general natural-recovery monitoring zone, comprised cells lacking the preceding risk and recovery characteristics. Zone 0 contained no continuously abandoned cropland in 2020 and served only as a cartographic and spatial-analysis background, not a formal management class. The Gi* result was used only as one of the two high-pressure criteria, together with upper-quartile RESDEN; it did not alter RC_CTX or the recovery-stage indicators.

The baseline decision order reflected management logic rather than a uniquely correct statistical classification. Among cells with ABAN_HA > 0, Zone 1 first identified the joint disadvantage of high residual pressure and weak RC_CTX; Zone 2 then identified concentrations of early-stage cropland exit on slopes ≥15°; Zone 3 captured the remaining high-pressure cells; and Zone 4 identified long-term exit combined with strong RC_CTX. All remaining positive-area cells entered Zone 5. Threshold sensitivity was evaluated using 20th/80th- and 30th/70th-percentile alternatives for RC_CTX, RESDEN, EARLYSTEEP and LONG10 while retaining ABAN_HA > 0 as the inclusion rule. Rule-order sensitivity was evaluated by moving the early-steep or general high-pressure rule earlier in the sequence. Exact classes and boundaries were treated as indicative and subject to local verification.

3. Results

3.1. Spatiotemporal Evolution and Event-Time Age Structure of Cropland Abandonment

From 2000 to 2020, the annual newly abandoned area and annual abandonment rate varied in parallel and showed pronounced interannual fluctuations (Figure 3a). New abandonment remained relatively high during 2000–2007, with local maxima in 2003 and 2006. Both metrics generally declined during 2008–2011, apart from a brief rebound in 2009. They rose again in 2012, remained comparatively low with minor fluctuations during 2013–2018, and increased sharply to a study period maximum in 2019. Although both declined in 2020, they remained above most values observed during 2013–2018. Thus, withdrawal from active cultivation did not follow a unidirectional trend but alternated between periods of expansion and contraction.

https://doi.org/10.3390/agronomy16191881

Cropland-exit event-anchor years formed a patchy and spatially heterogeneous pattern (Figure 3b). Early, intermediate and recent events occurred as scattered pixels and small patches embedded within cropland-dominated areas rather than as separate, extensive zones. Their spatial interspersion shows that exits from cultivation continued throughout the study period and accumulated locally. Recently abandoned cropland also remained dispersed in small patches, with no region-wide direction of expansion.

In 2020, *Age* formed a spatial mosaic across continuously abandoned cropland, with patches of different durations interspersed (Figure 3c). Land with Age >10 accounted for 48.91% of the total continuously abandoned area, the largest share; the Ages 1–3, 7–10 and 4–6 groups accounted for 22.87%, 14.82% and 13.40%, respectively. Long-term abandonment therefore dominated the 2020 stock, while the substantial share of recent abandonment indicated continuing renewal alongside temporal accumulation.

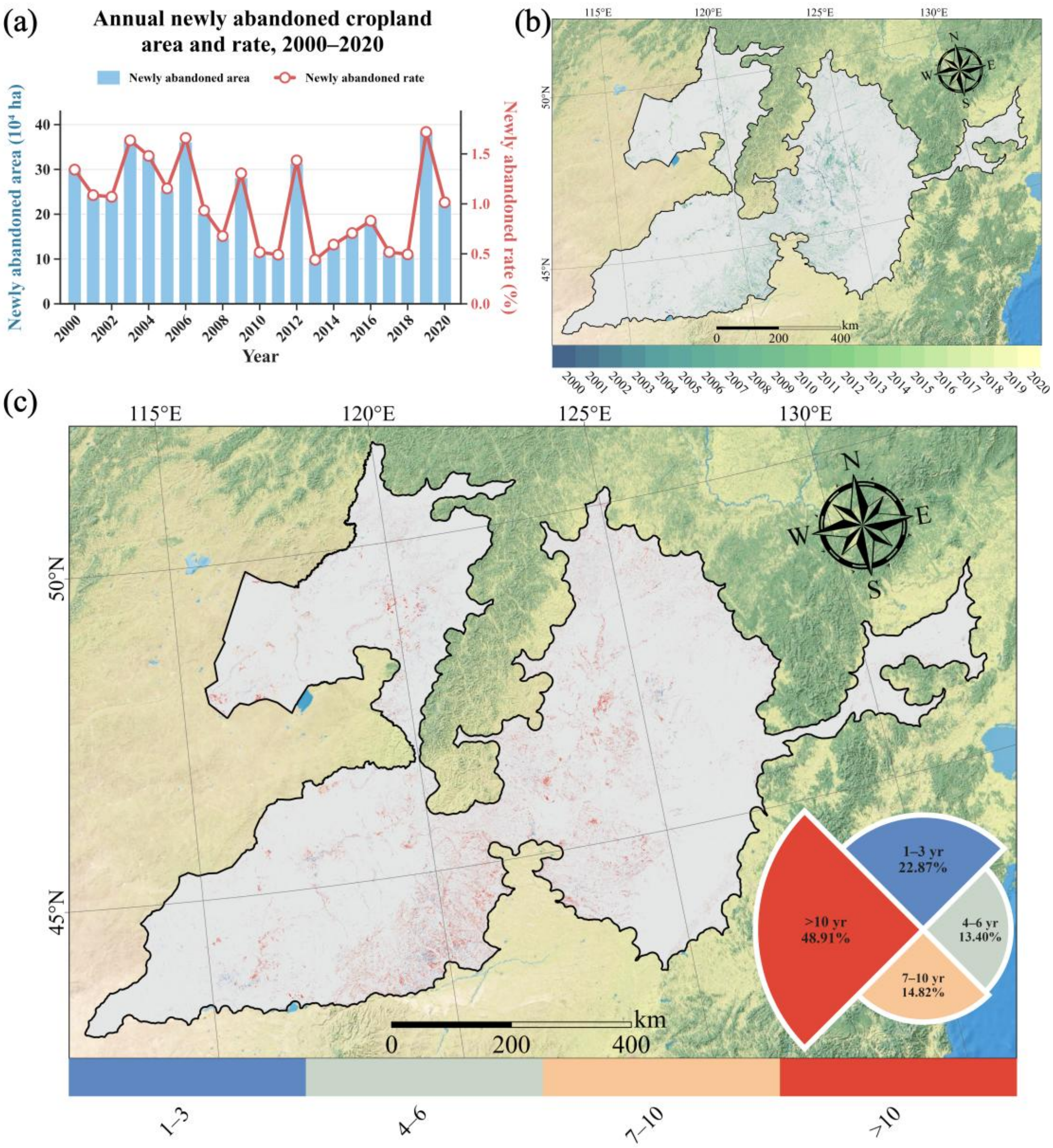

Figure 3. Spatiotemporal dynamics and event-time Age structure of cropland abandonment in the Northeast China black soil region from 2000 to 2020. (**a**) Interannual changes in the area and rate of newly abandoned cropland; (**b**) spatial distribution of the cropland-exit event-anchor year; and (**c**) spatial pattern and area proportions of the four event-time Age groups in 2020.

3.2. RUSLE-Based Hillslope Water Erosion Contrasts Across Event-Time Age Relative to Local Continuously Cultivated Cropland

The pre-event balance diagnostic retained 37,014,331 treatment-pixel observations and 532,909,654 assigned-control observations, representing 97.06% of the original eligible Age 1 treatments and 98.71% of assigned controls. At t − 2, the treatment–control difference in modelled erosion was 0.0373 t ha^{-1} yr^{-1} (SMD = 0.0369); at t − 1, it was 0.0166 t ha^{-1} yr^{-1} (SMD = 0.0164), and both the event-year and 20 km spatial-block confidence intervals crossed zero. The two-period change difference was −0.0206 t ha^{-1} yr^{-1} (SMD = −0.0438). Its event-year interval crossed zero, whereas the spatial-block interval was −0.0247 to −0.0167 t ha^{-1} yr^{-1}. All absolute SMDs were <0.10. Future-abandoned and local cultivated pixels therefore had generally similar pre-event modelled erosion, especially at t − 1, although a small spatially structured pre-trend and unobserved confounding remained. The diagnostic supports the use of local controls; it is not sufficient for causal identification.

Continuously abandoned cropland generally exhibited lower modelled hillslope water erosion than nearby continuously cultivated cropland, but the contrast developed in distinct stages. At the event anchor (Age 1), which is the last complete year in which the pixel was still classified as cropland, the estimated relative reduction metric was only 2.13%, and the intensity difference from the local control was small. By the first complete post-exit year (Age 2), the metric had increased to 40.56%, and the intensity difference widened markedly. This pattern was consistent with the rapid emergence of lower modelled erosion relative to local cultivated controls.

Because the pooled estimates above already describe the event-anchor and post-exit contrasts, the study next quantified their uncertainty directly. The cluster bootstrap results separated the uncertain event-anchor contrast from the clearer response from Age 2. The Age 1 estimate was supported by an observation-year cluster 95% CI of −4.90% to 9.84% and a 20 km spatial-block 95% CI of −0.76% to 5.00%, both of which crossed zero, whereas the Age 2 estimate had intervals of 37.75% to 43.27% and 38.74% to 42.38%, both fully above zero. For ΔE, the Age 1 estimate of −0.0168 t ha^{-1} yr^{-1} had an observation-year 95% CI of −0.0845 to 0.0385 and a spatial-block 95% CI of −0.0396 to 0.0060; the Age 2 estimate of −0.3099 t ha^{-1} yr^{-1} had corresponding intervals of −0.3719 to −0.2652 and −0.3289 to −0.2914. Across Ages 4–17, the lower RC confidence limits remained at least 42.96% and 44.42% under the observation-year and spatial-block bootstraps, respectively, while the upper ΔE limits remained no higher than −0.2846 and −0.3430 t ha^{-1} yr^{-1}. Ages 20 and 21 were retained as descriptive results because they were represented by only two and one independent observation years, respectively; their narrow year-cluster intervals were not interpreted as higher precision.

The pathway-stratified analysis showed that pooling post-exit land cover types concealed a meaningful difference in response magnitude. Both the forest and grassland pathways met the operational stable response criterion from Age 2, but the forest pathway strengthened more: RC rose from 41.43% at Age 2 to 53.75% at Ages 4–6, 57.14% at Ages 7–10 and 61.47% at Age >10, with year-cluster bootstrap 95% confidence intervals of 36.35–46.17%, 49.54–57.16%, 54.53–59.33% and 59.94–63.32%, respectively. The grassland pathway followed a flatter trajectory, with RC of 33.67%, 39.65%, 36.85% and 38.94% over the same intervals and all intervals above zero. Initial pathway labels were highly persistent: 99.31% of observations at Age >10 remained forest and 94.57% remained grassland. The unused/barren pathway accounted for only about 0.16% of Age 2 treatment observations and was supported by a single independent observation year, so it is reported descriptively and is not used for formal inference.

The 3 × 3 sensitivity analysis of stable reduction timing showed that the baseline criterion of a 67% positive-RC proportion and three consecutive Ages was fully reproduced for the overall sample and all four slope classes, with zero Age-level mismatches. The slope-stratified result was unchanged across all nine criterion combinations: the criterion was met at Age 1 on 0–5° slopes and at Age 2 on 5–15°, 15–25° and >25° slopes. The overall result showed a one-year sensitivity only under the strictest 75% positive-RC threshold; at 60% and 67%, the establishment Age remained Age 1 regardless of whether two, three or four consecutive Ages were required, whereas at 75% it shifted consistently to Age 2. Because the positive-RC proportion at Age 1 was 71.43%, between 67% and 75%, this sensitivity arose from the proportion threshold rather than from the consecutive-Age requirement.

Observation-year standardisation gave the same pattern (Figure 4b). At Age 1, mean RC was 4.31%, the median was 1.98%, the standard deviation was 13.10%, and 71.43% of year–Age units had a positive value, indicating variation among observation years. At Age 2, mean reduction reached 42.18%, the median reached 42.04%, and 100% of units had RC > 0. Mean and median values remained similar thereafter, with the positive share at 100%. The post-Age-2 relative erosion contrast was therefore consistent among observation years and was not driven primarily by a few years or by years with larger samples.

Control-radius sensitivity showed that the main event-time trajectories were nearly unchanged across 500, 1000 and 1500 m. Across Ages 1–19, RC trajectories at 500 and 1500 m were highly correlated with the 1000 m baseline ($r = 0.9998$ and 0.9999), with maximum absolute deviations of 2.02 and 0.82 percentage points and complete sign agreement. The corresponding ΔE trajectories were similarly consistent ($r = 0.9991$ and 0.9999), with maximum absolute deviations of 0.0175 and 0.0084 t ha^{-1} yr^{-1}. RC at Age 1 was 4.15%, 2.13% and 1.99% at 500, 1000 and 1500 m, respectively; at Age 2 it was 41.35%, 40.56% and 40.71%. From Ages 4 to 17, RC ranged from 47.14% to 49.92%, 46.55% to 50.00% and 47.08% to 50.75%, respectively.

Control radius had a clearer effect on sample support. Valid-comparison coverage across the four Age groups was 88.93%, 86.25%, 81.32% and 74.80% at 500 m; 94.18%, 92.43%, 89.43% and 86.11% at 1000 m; and 96.03%, 94.70%, 92.47% and 90.45% at 1500 m. A smaller radius increased spatial proximity but reduced coverage because fewer local controls met the eligibility criteria. A larger radius increased coverage while relaxing the neighbourhood constraint. The 1000 m radius thus provided a practical balance between local comparability and sample support. The operational criterion first qualified at Age 1 under the 500- and 1000 m radii and at Age 2 under the 1500 m radius. At 1500 m, Age 1 still had RC > 0 and $\Delta E < 0$, but the proportion of positive Year–Age RC values was 66.67%, marginally below the 67% threshold. Given that Age 1 is the event anchor, this difference was not interpreted as a substantive shift in post-exit timing.

Across the four Age stages, area-weighted relative reduction was 28.28% at Ages 1–3, well below later values because the small event-anchor contrast (Age 1) was followed by larger post-exit contrasts at Ages 2 and 3. Reduction increased to 47.69% at Ages 4–6, 47.93% at Ages 7–10 and 49.03% at Age >10. The small differences among these three later stages indicate that the response had entered a stable maintenance phase by Age 4 (Figure 4c).

At Ages 1–3, modelled soil erosion intensity was 0.554 t ha^{-1} yr^{-1} on abandoned cropland and 0.773 t ha^{-1} yr^{-1} on local continuously cultivated cropland, giving a difference of −0.219 t ha^{-1} yr^{-1} (Figure 4d and Table 2). The difference widened to −0.371, −0.385 and −0.415 t ha^{-1} yr^{-1} in the Ages 4–6, 7–10 and >10 groups, respectively. Thus, the erosion intensity contrast generally increased with event-time Age and remained stable over intermediate to long durations.

https://doi.org/10.3390/agronomy16191881

Table 2. Modelled hillslope water erosion responses across Age groups relative to local continuously cultivated cropland.

Event-Time Age Group	Year-Age Units	Observation Years	Valid Comparison Coverage (%)	E_abandon (t ha^{-1} yr^{-1})	E_control (t ha^{-1} yr^{-1})	ΔE (t ha^{-1} yr^{-1})	RC (%)	Positive RC Share (%)
Ages 1–3	60	21	94.18	0.554	0.773	−0.219	28.28	90
Ages 4–6	51	18	92.43	0.407	0.777	−0.371	47.69	100
Ages 7–10	54	15	89.43	0.418	0.803	−0.385	47.93	100
Age >10	66	11	86.11	0.431	0.847	−0.415	49.03	100

The event-time response therefore comprised an initial adjustment, rapid emergence and subsequent stability, with the transition from the event anchor (Age 1) to the first complete post-exit year (Age 2) marking the principal emergence of a stable relative erosion contrast.

Taken together, the regional relative erosion reduction contrast was small and statistically uncertain at the event anchor (Age 1) and became clear and robust from the first complete post-exit year (Age 2) onward. Because Age 1 is the last year in which the pixel was still classified as cropland, the contrast at Age 1 reflects pre-exit conditions rather than a post-exit ecological response.

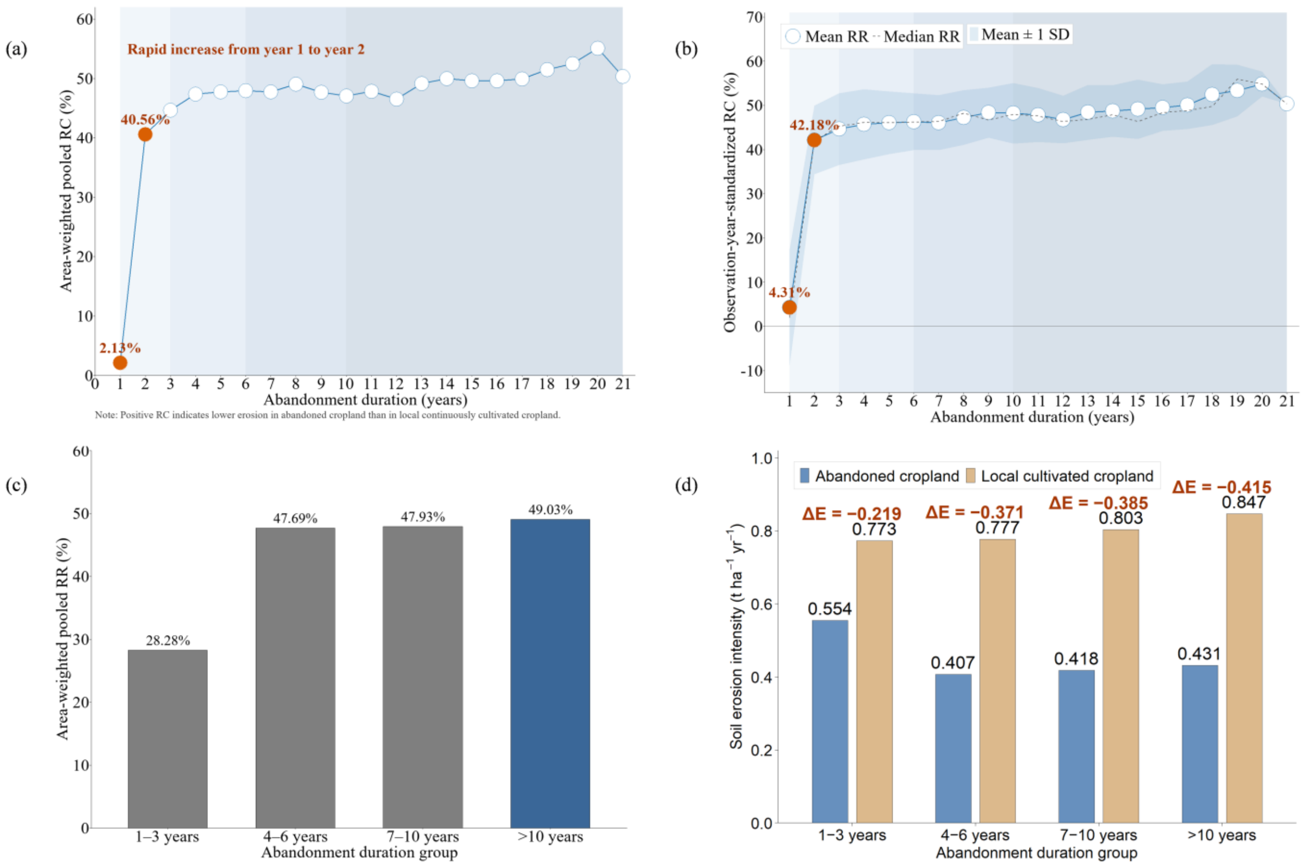

Figure 4. Modelled hillslope water erosion responses across event-time Age relative to local continuously cultivated cropland: (**a**) area-weighted pooled RC; (**b**) observation-year-standardised RC; (**c**) pooled RC by Age group; and (**d**) modelled hillslope water erosion intensity by Age group. All erosion quantities shown are RUSLE-based estimates.

3.3. Slope Dependence of the Event-Time RUSLE-Based Hillslope Water Erosion Response

Slope stratification revealed pronounced topographic variation in the erosion reduction response. The estimated relative erosion contrast became evident earlier and was larger on gentle slopes, whereas moderately steep and steep slopes showed weak or negative RC values at early event times before positive contrasts became evident. At Age 1, RC was 15.85% in the 0–5° class, whereas RC values were −22.84%, −63.50% and −45.75% in the 5–15°, 15–25° and >25° classes, respectively (Figure 5 and Table 3). At the event anchor, steeper land therefore did not exhibit a stable positive contrast relative to local continuously cultivated controls; this pre-exit difference is not evidence of a delayed post-exit ecological response. By Age 2, RC was positive in all four classes, reaching 47.77%, 26.19%, 6.45% and 17.10%, respectively.

Table 3. Event-time Age at which the operational stable relative erosion contrast was met, by slope class.

Slope Class	First Age with Positive Pooled Relative Reduction	First Age Meeting the Operational Stable Reduction Criterion
0–5°	1	1
5–15°	2	2
15–25°	2	2
>25°	2	2

Note: Age 1 is the cropland-exit event-anchor year (the last complete year classified as cropland); Age 2 is the first complete post-exit year. The criterion is an operational, sample-dependent descriptor and not a universal ecological threshold.

On gentle slopes, lower modelled erosion relative to local continuously cultivated cropland became evident earlier in event time, whereas steeper slopes showed negative contrasts at the event anchor before positive post-exit contrasts emerged. The 0–5° class retained the highest RC in every Age stage, with values of 37.57%, 53.74%, 54.24% and 54.87% for Ages 1–3, 4–6, 7–10 and >10, respectively (Figure 6a). The corresponding RR values for 5–15° were 10.16%, 34.32%, 34.59% and 37.43%. Reductions were smaller at 15–25° and >25°; within the Ages 1–3 group, RC was −17.84% and −3.58%, respectively, indicating that appreciable modelled erosion pressure persisted during early abandonment on moderately steep and steep land. RC became positive in both classes at Ages 4–6 but remained lower than in the 0–5° and 5–15° classes over the long term. The intensity difference ΔE was negative at every Age stage for the 0–5° and 5–15° classes, reaching ΔE values of −0.424 and −0.402 t ha^{-1} yr^{-1}, respectively, at Age >10 (Figure 6b). By contrast, the Ages 1–3 ΔE values were 0.207 and 0.024 t ha^{-1} yr^{-1} for 15–25° and >25°, turning negative at Ages 4–6 (−0.157 and −0.182 t ha^{-1} yr^{-1}, respectively).

Both the establishment time and the long-term magnitude of the estimated relative erosion contrast varied among slope classes. The advantage emerged early and remained strong on gentle slopes. Positive relative contrasts eventually became evident on moderately steep and steep land, but their magnitudes remained smaller than those on gentle slopes. This pattern identifies these terrain units as priorities during early abandonment.

Under same-fine-slope matching, the event-time structure was unchanged: the 0–5° class met the operational criterion from Age 1, whereas all six classes above 5° met it from Age 2. Age 2 RC was positive in every fine class (47.77%, 29.57%, 17.41%, 9.96%, 8.95%, 17.06% and 27.44% from 0–5° to ≥30°), whereas the Age 1 contrast varied strongly with terrain, from 15.85% at 0–5° to −64.11% at 20–25°. Exact magnitudes on steep terrain were more support-dependent: median Age-specific comparison coverage fell from 87.37% at

0–5° and 73.55% at 10–15° to 35.37% at 20–25° and 30.92% at 25–30°. The response therefore strengthened monotonically neither with slope nor with duration, and no simple linear slope dose–response is claimed.

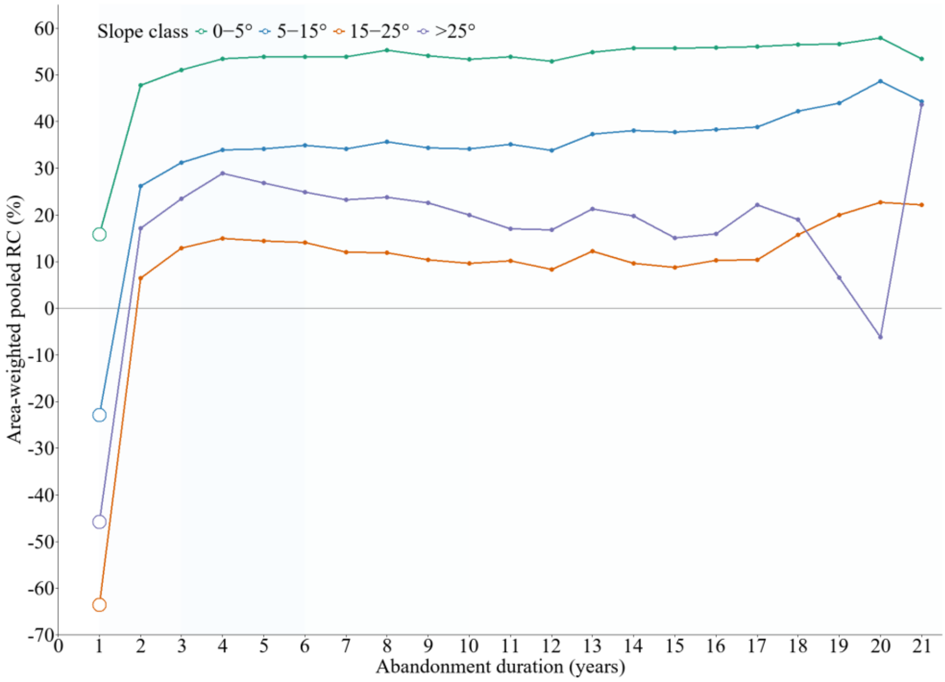

Figure 5. Pooled relative RUSLE-based hillslope water erosion reduction across event-time Age by slope class. The original horizontal-axis label "Abandonment duration (years)" denotes event-time Age, not elapsed years since abandonment: Age 1 is the cropland-exit event-anchor year (the last complete year classified as cropland), and Age 2 is the first complete post-exit year.

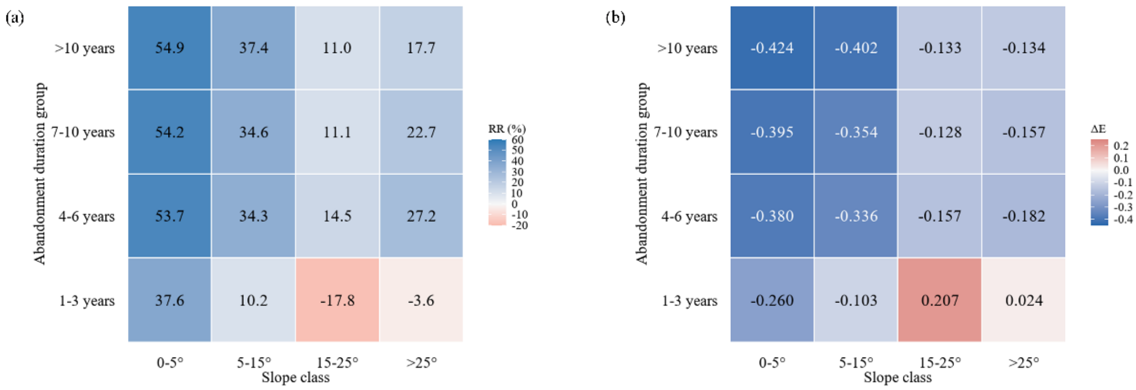

Figure 6. Modelled hillslope water erosion responses across slope classes and Age groups: (**a**) pooled relative reduction and (**b**) modelled erosion intensity difference between abandoned cropland and local continuously cultivated cropland.

3.4. Spatial Clustering of Residual Soil Loss and Differentiated Management Zones

In 2020, 6040 grid cells contained persistent cropland-exit area, totalling 2.148×10^6 ha and an estimated 1.090×10^6 t yr^{-1} of RUSLE-based residual hillslope water erosion. Residual soil loss density was strongly heterogeneous among grid cells (Figure 7a). Upper-quartile cells with $RSLD$ > 2.674 t km^{-2} yr^{-1} formed relatively continuous concentrations in the south and south-central region, with additional high-value patches in the east and north. Low values were widespread, showing that residual soil loss pressure did not scale uniformly with the spatial extent of abandonment.

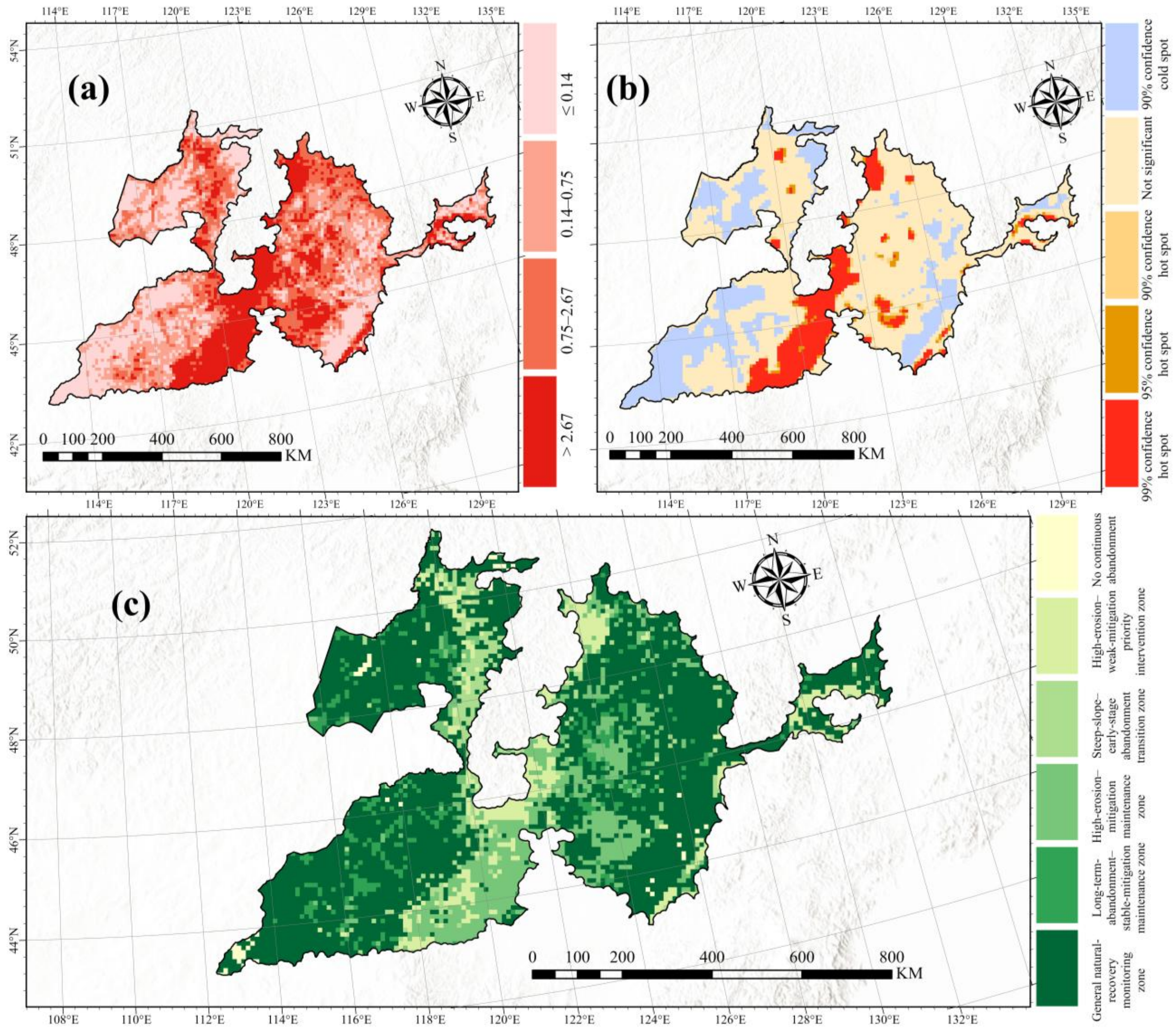

Figure 7. Modelled residual hillslope water erosion pressure, spatial clustering and indicative differentiated management zones for persistent cropland exit in 2020. (**a**) Residual soil loss density (RESDEN; t km^{-2} yr^{-1}); (**b**) baseline Getis–Ord Gi* hot and cold spots using a 15 km fixed-distance band; and (**c**) R2 rule-based indicative management zones.

Getis–Ord G_i^* analysis confirmed local clustering of high residual soil loss pressure (Figure 7b). Hot spots significant at the 95% or 99% confidence level comprised 922 grid cells, or 15.0% of all cells. They contained 40.6% of the continuously abandoned area but 55.5% of residual soil loss. Of these, 775 cells were significant at the 99% confidence level and contained 50.2% of total residual soil loss. A further 114 cells were hot spots at the 90% confidence level. Cold spots were detected only at the 90% confidence level and comprised 1362 cells. Residual soil loss was therefore more spatially concentrated than the continuously abandoned area.

Bandwidth and multiple-testing sensitivity supported the baseline hot spot pattern. At 10, 15 and 20 km distance bands, unadjusted 95% hot spots contained 50.06%, 55.54% and 57.09% of the regional ResidualSoilLoss, respectively. FDR correction reduced the number of 95% significant hot spots at 15 km to 738, but these cells still contained 48.69% of the regional load; the FDR-adjusted 99% hot spots contained 43.07%. Area-based Jaccard overlap between the 15 and 20 km results was 0.868 for the unadjusted 95% hot spots and 0.851 after FDR correction. Thus, multiple-testing correction and adjacent bandwidths altered the significant footprint but did not remove the concentration of high residual pressure.

Changing spatial support from 5 to 10 and 20 km conserved the total persistent cropland-exit area and regional ResidualSoilLoss but progressively smoothed their spatial concentration. The highest-RESDEN 20% of units contained 71.00%, 67.41% and 62.55% of the regional load at 5, 10 and 20 km, respectively; unadjusted 95% hot spots contained 58.79%, 55.54% and 49.72%. Area-based Jaccard overlap for 95% hot spots was 0.763 between 5 and 10 km and 0.723 between 10 and 20 km. The broad high-pressure pattern was therefore stable over the tested supports, although its concentration and exact boundaries were scale-dependent.

The rule set divided the 6040 grid cells containing continuously abandoned cropland into five management zones (Figure 7c and Table 4). The high residual soil loss–weak reduction priority intervention zone comprised 542 cells, 2.981 × 10^5 ha of continuously abandoned cropland and 3.089 × 10^5 t yr^{-1} of residual soil loss. It had the highest area-weighted mean modelled hillslope water erosion intensity (1.036 t ha^{-1} yr^{-1}), whereas RC_CTX was only 35.66%. The high residual soil loss–reduction maintenance zone comprised 800 cells and contained 8.441 × 10^5 ha of continuously abandoned cropland and 3.985 × 10^5 t yr^{-1} of residual soil loss, both larger than in any other zone. Together, the two high-loss zones represented 1342 cells, or 22.2% of cells with continuous abandonment, and contained 53.2% of the abandoned area and 64.9% of residual soil loss. They also included 778 hot spot cells significant at ≥95%, or 84.6% of the 920 high-confidence hot spots within abandonment-containing cells. These two zones therefore defined the principal spatial concentration of residual soil loss pressure.

Table 4. Summary statistics and indicative regional management priorities for the R2 zones.

Management Zone	Grid Cells (n)	Persistent Cropland-Exit Area (10^3 ha)	Residual Soil Loss (10^3 t yr^{-1})	Mean Modelled Hillslope Water Erosion Intensity (t ha^{-1} yr^{-1})	Class-Based Expected Relative Reduction Context, RC_CTX (%)	Indicative Regional Management Priority
High residual soil loss–weak reduction priority intervention zone	542	298.07	308.92	1.036	35.66	Prioritise hillslope protection, vegetation recovery and targeted soil and water conservation.
Steep-slope early-abandonment transition zone	1049	337.34	184.00	0.545	40.55	Intensify monitoring across event-time Ages 1–3 and stabilise moderately steep and steep abandoned slopes.
High residual soil loss–reduction maintenance zone	800	844.07	398.53	0.472	47.19	Maintain erosion reduction gains while controlling high-loss source areas.
Long-term abandonment–stable reduction maintenance zone	568	117.23	30.56	0.261	51.25	Maintain natural recovery and prevent renewed disturbance.
General natural-recovery monitoring zone	3081	551.38	168.31	0.305	46.68	Conduct routine monitoring of natural recovery.
Total	6040	2148.09	1090.31	0.508	44.64	—

The steep-slope early-abandonment transition zone and long-term abandonment–stable reduction maintenance zone comprised 1049 and 568 cells and contained 16.9% and

2.8% of total residual soil loss, respectively. The latter had the lowest area-weighted mean modelled hillslope water erosion intensity (0.261 t ha^{-1} yr^{-1}) and the highest RC_CTX (51.25%). The general natural-recovery monitoring zone contained 3081 cells, or 51.0% of cells with continuous abandonment, but only 15.4% of total residual soil loss. The dominance of this zone by grid count did not translate into a comparable share of the load, confirming that regional management demand was spatially concentrated.

Management-zone sensitivity showed that the exact classification was operational rather than universal. Under the 20th/80th- and 30th/70th-percentile schemes, zone-specific grid counts (continuously abandoned area, 10^3 ha; residual soil loss, 10^3 t yr^{-1}) varied as follows: Zone 1, 389–717 (192.28–407.58; 225.27–384.71); Zone 2, 884–1186 (267.87–412.54; 157.76–215.43); Zone 3, 754–837 (819.91–833.62; 348.34–437.77); Zone 4, 455–630 (112.98–116.89; 27.98–30.22); and Zone 5, 2670–3558 (395.08–737.44; 113.86–239.29). Relative to the 25th/75th-percentile baseline, the two alternatives changed 12.27% and 11.71% of cell assignments, while the combined intervention footprint of Zones 1 and 2 retained area-based Jaccard overlaps of 0.794 and 0.829. Alternative rule orders changed 3.54–7.63% of zone labels. These tests supported the broad location of priority areas but showed that exact zone membership and boundaries depend on the percentile scheme and rule sequence.

4. Discussion

4.1. Temporal Development and Possible Mechanisms Underlying the Abandonment-Associated Erosion Response

Lower modelled erosion relative to local continuously cultivated controls was small and statistically uncertain at Age 1 (2.13%), which represents the event-anchor year and the last complete year in which the pixel was classified as cropland. The contrast increased to 40.56% at Age 2, the first complete post-exit year, and remained at approximately 47–50% during Ages 4–17. The near-zero contrast at Age 1 is consistent with its role as an event-time reference and should not be interpreted as a weak first-year ecological response to abandonment. Instead, the change between Ages 1 and 2 marks the first observed contrast following cropland exit. From Age 2 onward, the sustained relative contrast is consistent with changes in vegetation cover, litter accumulation and surface conditions after cultivation ceased. These changes may reduce raindrop impact and overland flow, while improvements in soil structure and infiltration may develop more slowly. However, vegetation, roots, soil aggregates and infiltration were not measured directly; these mechanisms therefore remain interpretations requiring field validation.

Because the forest and grassland pathways share the same non-cropland status but follow different relative reduction trajectories, the event-time pattern cannot be a direct mechanical reflection of the land cover class transition alone. The contrast between pathways nevertheless remains partly confounded with the shared land cover information that enters both event identification and the CSWED C and P factors, so it is interpreted as pathway-associated heterogeneity in a modelled response rather than as a mechanism independent of the land cover data.

4.2. Slope Dependence of the Abandonment-Associated Erosion Response

Event-time Age was not the sole determinant of the erosion response. Both the establishment and long-term magnitude of the estimated relative erosion contrast varied among slope classes. The operational stable reduction criterion was met at the event anchor (Age 1) on 0–5° slopes but generally from the first complete post-exit year (Age 2) on 5–15°, 15–25° and >25° slopes, and the early advantage was markedly weaker on moderately steep and steep land. The statistical erosion response associated with abandonment was therefore terrain-dependent: land with the same event-time Age could occupy different recovery states under different topographic forcing.

This contrast may reflect competition between recovering surface protection and the erosive power of hillslope flow. On gentle slopes, lower runoff velocity and transport capacity may allow vegetation recovery, litter accumulation and increasing surface roughness to be associated with a larger erosion contrast. As slope increases, greater flow energy and sediment-transport capacity may exceed the protection supplied by sparse early vegetation and immature roots. The 15–25° and >25° classes consequently retained weak relative reductions at Ages 1–3 and shifted towards stable reduction only as recovery continued. Their long-term relative reduction estimates also remained below those on gentle slopes, indicating that steeper terrain was associated with a later and smaller relative response.

Slope dependence also helps reconcile apparently divergent evidence from abandoned-land studies. Cessation of cultivation and vegetation recovery generally reduce runoff and soil loss, but the direction and magnitude vary across environmental settings [16,21,38,39]. In Mediterranean mountain catchments, cultivation history, subsequent land use and terrain can dampen differences in soil redistribution among vegetation states. On abandoned Loess Plateau terraces, concentrated flow and deteriorating engineering structures can maintain high erosion risk when maintenance ceases or extreme rainfall occurs [16]. Our results are consistent with an overall pattern of lower modelled hillslope water erosion on persistently exited cropland than on locally continuously cultivated controls. The estimates indicate that the statistical response has a definable establishment phase and varies systematically among slope classes: it is a dynamic outcome of event-time Age interacting with slope, not a fixed attribute of abandoned land. Classifying soil-retention status from abandonment alone would therefore be inadequate; recovery stage and terrain must be evaluated together.

The event-time trajectory observed here can also be compared with abandonment and restoration studies from other regions, most of which emphasise the timing of the response rather than only its direction. Reported trajectories range from rapid responses where ground cover re-establishes within one or two growing seasons, to delayed responses of a decade or more where succession is slow, grazing or fire intervenes, or terraces and drainage structures degrade after maintenance ceases [4,14,16,21,40]. Where sites are compared only as abandoned versus cultivated, this range of lag times is averaged away. The Northeast China trajectory reported here—a contrast that is small at the event anchor, clear from the first complete post-exit year, and then near-stable—is consistent with rapid re-establishment of surface cover on these sloping Mollisols, but it should not be transferred directly to other environmental settings, because the timing depends on climate, successional pathway, terrain and prior management history.

4.3. Spatial Differentiation of Residual Soil Loss and Priorities for Black Soil Conservation

An erosion reduction advantage relative to local continuously cultivated cropland did not eliminate absolute modelled soil loss pressure. In 2020, the two high-loss zones represented 22.2% of cells containing persistent cropland-exit area but accounted for 64.9% of RUSLE-based residual hillslope water erosion. This spatial asymmetry indicates that allocation in proportion to exited area alone would overlook major modelled loss sources. Regional prioritisation should instead consider absolute pressure together with recovery stage, slope and class-based relative reduction context, while recognizing that these variables describe an observational, model-dependent screening framework rather than measured local treatment effects.

The zones suggest distinct, but provisional, conservation pathways. Cells with high modelled residual loss and weak RC_CTX may warrant field assessment for vegetation recovery, hillslope runoff control and targeted soil and water conservation [20,22,24]. Cells with high residual loss but a stronger expected reduction context contain extensive persistent cropland-exit area, so maintaining recovery while locating persistent source areas is more informative than asking only whether relative erosion is lower. Early-stage exit on slopes ≥15° warrants closer surveillance of vegetation cover, residual bare ground and concentrated flow, whereas long-term exit with a strong expected context may be managed by avoiding renewed disturbance [4,5,21]. Lower-pressure areas are better suited to periodic remote-sensing surveillance [6,41,42]. Because the percentile cut-offs are study-area-relative operational thresholds, these pathways are indicative priorities rather than universal prescriptions and require local confirmation before implementation.

Getis–Ord G_i^* hot spots and the rule-based zones supplied complementary spatial evidence for this differentiation. High residual soil loss clustered in distinct neighbourhoods rather than occurring randomly, so management demand may extend across individual grid cells and administrative boundaries. Zoning then combined each cell's soil loss status with its recovery context to assign the form and priority of intervention. Effective black soil conservation must therefore identify spatial clusters of high loss while distinguishing recovery stages and relative reduction states within them, rather than ranking areas from a single erosion metric or the extent of abandonment. In this core grain-producing region, scarce conservation resources should be directed towards loss sources that most threaten the black soil layer and future productive capacity, while allowing recovery to continue where a stable long-term relative erosion contrast is already evident.

The sensitivity analyses qualified the spatial management interpretation without overturning its central pattern. The concentration of high residual erosion pressure persisted across distance band and false discovery rate adjustments, whereas aggregation to coarser grids weakened load concentration. Exact management assignments were more sensitive to analytical support than the broad hot spot footprint, and alternative thresholds and rule orders mainly reassigned marginal cells. The resulting maps should therefore support regional screening and cross-boundary coordination rather than be interpreted as fixed field-level governance units.

Several limitations bound the causal interpretation. Comparing abandoned pixels with local contemporaneous continuously cultivated controls and stratifying the analysis by slope improved spatial and terrain comparability, but abandonment was not randomly assigned. Unobserved variation in soil properties and prior soil degradation, historical tillage and conservation practices, drainage, field accessibility, distance to settlements and roads, land quality, and local socioeconomic or policy conditions could affect both the probability of abandonment and modelled erosion. Information on management within the cultivated controls—including tillage, residue retention, mulching, reduced tillage, contouring, and ridge orientation—was also unavailable at a resolution compatible with the 30 m annual analysis. The estimated differences therefore represent statistical associations with continuous cropland abandonment rather than isolated causal effects [4,5].

The erosion response was derived from the CSWED RUSLE product rather than directly measured in this study. The response variable is therefore not a field-based erosion measurement; the analysis uses a published 30 m annual modelled product, and this is stated explicitly throughout the manuscript. Although the source product was evaluated against provincial water erosion statistics reported in the China Soil and Water Conservation Bulletins and against observations from 446 runoff plots, that evaluation was carried out by the source study at the national scale. It is therefore a source-product validation and does not constitute a new field validation conducted here for abandoned cropland in Northeast China's black soil region [32]. RUSLE represents rainfall–runoff-driven interrill and rill erosion but does not quantify gully, wind, or freeze–thaw erosion. The CSWED C factor combines CLCD land cover classes with Landsat-derived NDVI and fractional vegetation cover, and the P factor uses land cover together with slope, so the exposure definition and the modelled response share part of their land cover information. CLCD land cover information contributed both to identifying continuous abandonment and to estimating the C factor, and partly to the P factor, creating information coupling between the exposure definition and the modelled response. Because the same classification product feeds both pathways, the resulting uncertainties are not independent, which further limits any attempt to partition the total uncertainty of the estimated relative contrast. The source product reports Geodetector (v6.1.5) q values for Northeast China of 0.115 for R, 0.033 for K, 0.423 for LS, 0.136 for C and 0.365 for P, indicating that LS and P explain most of the spatial variation in modelled erosion. These q values quantify explanatory contribution and are not an error propagation analysis. Uncertainty in the R, K, LS, C, and P factors and their covariance was not formally propagated [43,44]. The slope variable used for stratification was derived from the Copernicus DEM GLO-30 and is conceptually distinct from the LS factor embedded within CSWED. Slope-stratified contrasts therefore reflect both genuine terrain-related differences in the abandonment response and the structural slope sensitivity of the RUSLE LS parameterisation, and the latter is likely to matter most on steep terrain where DEM-derived slope and LS estimates are also more uncertain. The results are therefore not treated as deterministic truth. Because consistent annual R, K, LS, C and P rasters and their joint error distributions are not available, factor-level sensitivity experiments were not attempted, and arbitrary fixed-percentage perturbations of the final erosion map would not represent the uncertainty structure of the source model. The regional residual soil loss total should consequently be interpreted as a model-based estimate rather than an error-free measurement.

Dependence among event-time observations and the spatial–temporal scope of the analysis further constrain generalisation. Some abandonment cohorts contributed observations to multiple Age classes, while the number of independent calendar-year observations declined toward larger event-time Ages. The resulting establishment time is therefore an operational, sample- and criterion-dependent descriptor rather than a universal ecological threshold. Climate variability is partly represented in the analysis. The CSWED rainfall erosivity factor varies annually and is derived from station-based precipitation interpolated to 30 m using a random forest model with an interpolation R^2 of approximately 0.92, so interannual rainfall differences enter the RUSLE calculation explicitly. In addition, the comparison uses contemporaneously cultivated local controls, which removes much of the large-scale interannual rainfall signal from the relative contrast. However, an annual erosivity factor cannot resolve short-duration extreme rainfall events, and the source product also reports pronounced erosion peaks in some extreme years; the analysis should therefore be read as accounting for interannual rainfall variation but not for short-duration extremes. Residual soil loss in 2020 represents a single end-of-period state, and future climate change and extreme rainfall may alter both erosion pressure and conservation performance [45]. The 10 km grid was appropriate for regional zoning but inevitably smoothed field- and hillslope-scale heterogeneity, while erosion patterns and their drivers are themselves scale-dependent [33,45]. Long-term field plots, coupled vegetation–soil process observations, finer-scale validation, and dynamic erosion monitoring are needed to test the inferred establishment process and refine the management zones.

4.4. Study Limitations and Scope of Inference

Several limitations constrain causal interpretation. The local-control design aligned observation year, neighbourhood, continued cultivation and, in slope-stratified analyses, terrain class, while the pre-event diagnostic indicated generally small modelled erosion differences before the event. These safeguards did not eliminate unobserved confounding

https://doi.org/10.3390/agronomy16191881

because abandonment was not randomly assigned. Initial soil fertility, soil texture, compaction, drainage, accessibility, productivity, historical management, conservation practices, local policy and proximity to infrastructure may affect both cropland exit and modelled erosion. Region-wide annual information on tillage, residue management, mulching, conservation tillage, ridge orientation and contour farming was unavailable at a resolution compatible with the 30 m analysis. The estimates therefore represent abandonment-associated statistical contrasts with local cultivated controls rather than causal treatment effects [4,5].

Dependence among event-time observations also requires qualification. The same abandoned pixel could contribute observations to multiple Age classes across observation years. The observation-year bootstrap retained all Age units within each resampled year, whereas the 20 km spatial-block bootstrap retained all years and Ages within each resampled block, thereby preserving repeated spatial contributions. These procedures characterise uncertainty associated with year/cohort composition and spatial clustering but do not establish causal identification. Getis–Ord Gi* addressed only the neighbourhood clustering of RESDEN and was not used to quantify uncertainty in RC or ΔE.

The erosion response was derived from CSWED RUSLE estimates rather than direct measurements. The source product was evaluated nationally against provincial water erosion statistics (five-year mean absolute error, 9.48%) and observations from 446 runoff plots, but this does not constitute field validation for abandoned cropland in Northeast China's black soil region [32]. RUSLE represents rainfall–runoff-driven interrill and rill erosion and excludes gully, wind and freeze–thaw erosion. Because CLCD contributes both to abandonment identification and to the CSWED C factor, and partly to the P factor, the exposure and response share land cover information. The cluster bootstraps do not propagate the joint uncertainty or covariance of CLCD classification and the R, K, LS, C and P factors; compatible annual factor-level error distributions were unavailable [43,44]. The source product's Geodetector q values describe explanatory contributions rather than factor-level error distributions. Moreover, the Copernicus-derived slope used for stratification is conceptually distinct from the LS factor embedded in CSWED, so steep-slope contrasts combine terrain-related response heterogeneity with the structural slope sensitivity of RUSLE. The regional residual soil loss total should therefore be interpreted as a model-based estimate, not an error-free measurement.

The establishment rule and management thresholds are operational and study-area-relative. Residual soil loss in 2020 is a single end-of-period state, the 10 km grid smooths field- and hillslope-scale heterogeneity, and exact hot spot and management-zone boundaries depend partly on analytical support. Annual rainfall erosivity captures interannual variability but not short-duration extreme events, while future climate change may alter erosion pressure and conservation performance [45]. Long-term field plots, coupled vegetation–soil observations, finer-scale validation and dynamic erosion monitoring are therefore required before regional priorities are translated into site-specific interventions [33,45].

5. Conclusions

Annual land cover trajectories and comparisons with local contemporaneous continuously cultivated controls revealed a strongly time-dependent statistical association between continuous cropland abandonment and lower RUSLE-based hillslope water erosion in Northeast China's black soil region. The relative reduction metric was small and statistically uncertain at the cropland-exit event anchor (Age 1; RR = 2.13%, with both cluster-bootstrap 95% confidence intervals including zero), increased to 40.56% in the first complete post-exit year (Age 2, with both intervals above zero), and remained at approximately 47–50% during Ages 4–17. The operational stable reduction criterion was met from Age 1 on 0–5° slopes but generally from Age 2 on steeper land, with smaller early and long-term contrasts on moderately steep and steep slopes. These estimates describe abandonment-associated differences relative to local cultivated controls rather than an isolated causal effect.

Lower relative erosion did not eliminate substantial absolute soil loss pressure. In 2020, the 6040 baseline 10 km × 10 km cells containing continuously abandoned cropland carried an estimated 1.090×10^6 t yr^{-1} of residual RUSLE-based hillslope water erosion. Under the baseline 15 km Getis–Ord Gi* analysis, hot spots significant at the 95% or 99% confidence level occupied 15.0% of the cells but contained 55.5% of the residual loss; the two management zones defined by high residual pressure occupied 22.2% of the cells and contained 64.9% of the total. Sensitivity analyses retained this broad spatial concentration, although exact hot spot and management-zone boundaries varied with grid support, distance band, multiple-testing adjustment, thresholds, and rule order. The framework therefore supports prioritizing recently abandoned land on moderately steep and steep slopes and spatially concentrated high-loss areas, while maintaining recovery conditions where a stable long-term erosion contrast is already evident. The percentile cut-offs used to define the zones are study-area-relative, data-driven operational thresholds rather than universal ecological or management thresholds, and the absence of region-specific long-term plot- or pixel-scale field validation in Northeast China's black soil region remains a limitation of this assessment. These priorities should be treated as indicative regional screening results rather than fixed field-level governance units and require local validation; they do not extend to gully, wind, or freeze–thaw erosion. Within these bounds, the event-time- and slope-explicit framework directs conservation resources toward areas where continuous abandonment has not yet produced a substantial relative reduction or where absolute modelled soil loss remains high.

Funding: This research is supported by the Project of the National Natural Science Foundation of China (grant number: 42071233).

Data Availability Statement: The original contributions presented in this study are included in the article. Further inquiries can be directed to the corresponding author.

Acknowledgments: The author gratefully acknowledges the editorial team and the anonymous peer reviewers for their time, expertise, and thorough assessment. Their critical feedback and thoughtful recommendations were instrumental in strengthening the final version of this work.

Conflicts of Interest: The author declares no conflicts of interest.

References

1. Zhao, J.; Zhang, Z.; Zhao, C.; Liu, Z.; Guo, E.; Zhang, T.; Chen, J.; Olesen, J.E.; Liu, K.; Harrison, M.T.; et al. Dissecting the vital role of dietary changes in food security assessment under climate change. *Commun. Earth Environ.* **2024**, *5*, 440. https://doi.org/10.1038/s43247-024-01612-3.
2. Moallemi, E.A.; Castonguay, A.C.; Mason-D'Croz, D.; Nelson, R.; Britz, W.; Allen, C.; Hadjikakou, M.; Battaglia, M.; Bryan, B.A.; Conti, C.; et al. Complexity and uncertainty in future food system transformation modelling. *Nat. Food* **2025**, *6*, 1008–1019. https://doi.org/10.1038/s43016-025-01257-1.
3. Liu, T.; Yu, L.; Liu, X.; Peng, D.; Chen, X.; Du, Z.; Tu, Y.; Wu, H.; Zhao, Q. A global review of monitoring cropland abandonment using remote sensing: Temporal–spatial patterns, causes, ecological effects, and future prospects. *J. Remote Sens.* **2025**, *5*, 0584. https://doi.org/10.34133/remotesensing.0584.
4. Fayet, C.M.; Reilly, K.H.; Van Ham, C.; Verburg, P.H. What is the future of abandoned agricultural lands? A systematic review of alternative trajectories in Europe. *Land Use Policy* **2022**, *112*, 105833. https://doi.org/10.1016/j.landusepol.2021.105833.
5. Subedi, Y.R.; Kristiansen, P.; Cacho, O. Drivers and consequences of agricultural land abandonment and its reutilisation pathways: A systematic review. *Environ. Dev.* **2022**, *42*, 100681. https://doi.org/10.1016/j.envdev.2021.100681.

6. Prishchepov, A.V.; Anders, K.; Feranec, J.; Goga, T.; Gradinaru, S.R.; Kolář, J.; Pazur, R.; Potůčková, M.; Zagajewski, B.; Kupková, L. The progress and potential directions in the remote sensing of farmland abandonment. *Remote Sens. Environ.* **2025**, *331*, 115019. https://doi.org/10.1016/j.rse.2025.115019.
7. Zhang, M.; Li, G.; He, T.; Zhai, G.; Guo, A.; Chen, H.; Wu, C. Reveal the severe spatial and temporal patterns of abandoned cropland in China over the past 30 years. *Sci. Total Environ.* **2023**, *857*, 159591. https://doi.org/10.1016/j.scitotenv.2022.159591.
8. Li, T.; Liu, C.; Wang, Y. Continuous monitoring of cropland abandonment in China since the 21st century: Interpreting spatio-temporal trajectories and characteristics. *Land* **2025**, *14*, 2203. https://doi.org/10.3390/land14112203.
9. Liu, X.; Wang, S.; Zhang, X.; Zhen, L.; Ma, C.; Naing, S.Y.; Liu, K.; Li, H. Monitoring spatiotemporal dynamics of farmland abandonment and recultivation using phenological metrics. *Land* **2025**, *14*, 1745. https://doi.org/10.3390/land14091745.
10. Zhang, X.; Chen, X.; Yuan, L. Asynchronous soil-hydrological and landscape responses to dynamic cropland abandonment in Northeast China. *CATENA* **2026**, *274*, 110500. https://doi.org/10.1016/j.catena.2026.110500.
11. Tian, P.; Tian, X.; Geng, R.; Zhao, G.; Yang, L.; Mu, X.; Gao, P.; Sun, W.; Liu, Y. Response of soil erosion to vegetation restoration and terracing on the Loess Plateau. *CATENA* **2023**, *227*, 107103. https://doi.org/10.1016/j.catena.2023.107103.
12. Qiu, D.; Xu, R.; Wu, C.; Mu, X.; Zhao, G.; Gao, P. Vegetation restoration improves soil hydrological properties by regulating soil physicochemical properties in the Loess Plateau, China. *J. Hydrol.* **2022**, *609*, 127730. https://doi.org/10.1016/j.jhydrol.2022.127730.
13. Han, C.; Song, M.; Tang, Q.; Wei, J.; He, X.; Collins, A.L. Post-farming land restoration schemes exhibit higher soil aggregate stability and organic carbon: Evidence in the Three Gorges Reservoir Area, China. *CATENA* **2023**, *227*, 107099. https://doi.org/10.1016/j.catena.2023.107099.
14. Cammeraat, E.; Anders, N.; Scholten, R.; Boix-Fayos, C. Erosion and sedimentation on an abandoned terraced and gullied hillslope. *CATENA* **2024**, *246*, 108393. https://doi.org/10.1016/j.catena.2024.108393.
15. Lv, X.; Tang, Q.; Han, C.; Song, M.; Yuan, C.; Yang, Q.; Wei, J.; He, X.; Collins, A.L. Farmland abandonment and vegetation succession mediate soil properties but are determined by the duration of conversion. *CATENA* **2024**, *238*, 107877. https://doi.org/10.1016/j.catena.2024.107877.
16. Fang, X.; Peng, M.; Yan, Y.; Xu, X.; Na, J. Runoff–sediment dynamics and degradation patterns in an abandoned terraced landscape on the Loess Plateau. *Earth Surf. Process. Landf.* **2024**, *49*, 4202–4212. https://doi.org/10.1002/esp.5960.
17. Liu, Y.; Liu, G.; Gu, J.; Shi, H.; Li, H.; Han, Y.; Liu, D.; Xia, X.; Guo, Z. Soil erodibility and hillslope erosion processes affected by vegetation restoration duration. *Soil Tillage Res.* **2025**, *245*, 106305. https://doi.org/10.1016/j.still.2024.106305.
18. Hong, C.; Prishchepov, A.V.; Bavorova, M. Cropland abandonment in mountainous China: Patterns and determinants at multiple scales and policy implications. *Land Use Policy* **2024**, *145*, 107292. https://doi.org/10.1016/j.landusepol.2024.107292.
19. Xu, Y.; Luo, L.; Guo, W.; Jin, Z.; Tian, P.; Wang, W. Revegetation changes main erosion type on the gully–slope on the Chinese Loess Plateau under extreme rainfall: Reducing gully erosion and promoting shallow landslides. *Water Resour. Res.* **2024**, *60*, e2023WR036307. https://doi.org/10.1029/2023wr036307.
20. Huang, D.; Zhao, X.; Yin, Z.; Qin, W. Utilizing geodetectors to identify conditioning factors for gully erosion risk in the black soil region of northeast China. *Int. Soil Water Conserv. Res.* **2024**, *12*, 808–827. https://doi.org/10.1016/j.iswcr.2024.07.004.
21. Khorchani, M.; Gaspar, L.; Nadal-Romero, E.; Arnaez, J.; Lasanta, T.; Navas, A. Effects of cropland abandonment and afforestation on soil redistribution in a small Mediterranean mountain catchment. *Int. Soil Water Conserv. Res.* **2023**, *11*, 339–352. https://doi.org/10.1016/j.iswcr.2022.10.001.
22. Zhang, X.; Song, J.; Wang, Y.; Sun, H.; Li, Q. Threshold effects of vegetation coverage on runoff and soil loss in the Loess Plateau of China: A meta-analysis. *Geoderma* **2022**, *412*, 115720. https://doi.org/10.1016/j.geoderma.2022.115720.
23. Wang, H.; Yang, S.; Wang, Y.; Gu, Z.; Xiong, S.; Huang, X.; Sun, M.; Zhang, S.; Guo, L.; Cui, J.; et al. Rates and causes of black soil erosion in Northeast China. *CATENA* **2022**, *214*, 106250. https://doi.org/10.1016/j.catena.2022.106250.
24. Rajbanshi, J.; Das, S.; Paul, R. Quantification of the effects of conservation practices on surface runoff and soil erosion in croplands and their trade-off: A meta-analysis. *Sci. Total Environ.* **2023**, *864*, 161015. https://doi.org/10.1016/j.scitotenv.2022.161015.
25. Duan, X.; Xie, Y.; Ou, T.; Lu, H. Effects of soil erosion on long-term soil productivity in the black soil region of northeastern China. *CATENA* **2011**, *87*, 268–275. https://doi.org/10.1016/j.catena.2011.06.012.
26. Zhang, J.; Wang, M.; Liu, K.; Zhao, Z. Dynamic changes in soil erosion and challenges to grain productivity in the black soil region of Northeast China. *Ecol. Indic.* **2025**, *171*, 113145. https://doi.org/10.1016/j.ecolind.2025.113145.

27. Gu, Z.; Xie, Y.; Gao, Y.; Ren, X.; Cheng, C.; Wang, S. Quantitative assessment of soil productivity and predicted impacts of water erosion in the black soil region of northeastern China. *Sci. Total Environ.* **2018**, *637–638*, 706–716. https://doi.org/10.1016/j.scitotenv.2018.05.061.
28. Chen, Q.; Zhang, J.; Guo, M.; Zhang, X.; Tian, J.; Zhou, P.; Chen, Z. Comparison of the effects of five long-term land use and management practices on runoff, soil erosion, and nutrient loss under natural rainfall in the Mollisol region of Northeast China. *Earth Surf. Process. Landf.* **2024**, *49*, 1606–1620. https://doi.org/10.1002/esp.5789.
29. Wang, X.; Zheng, F.; Liang, R.; Yang, X.; Mo, S.; An, X. Effects of spatial distribution of slope erosion-deposition on soil quality degradation in the Mollisol region of Northeast China. *Soil Tillage Res.* **2026**, *257*, 106966. https://doi.org/10.1016/j.still.2025.106966.
30. Yang, J.; Huang, X. The 30 m Annual Land Cover Datasets and its Dynamics in China from 1985 to 2025, Version 1.0.5. *Zenodo* **2026**, https://doi.org/10.5281/zenodo.18180184.
31. Getis, A.; Ord, J.K. The analysis of spatial association by use of distance statistics. *Geogr. Anal.* **1992**, *24*, 189–206. https://doi.org/10.1111/j.1538-4632.1992.tb00261.x.
32. Yan, J.; Wang, S.; Feng, J.; He, H.; Wang, L.; Sun, Z.; Zheng, C. New 30-m resolution dataset reveals declining soil erosion with regional increases across Chinese mainland (1990–2022). *Remote Sens. Environ.* **2025**, *323*, 114681. https://doi.org/10.1016/j.rse.2025.114681.
33. Liu, B.; Zhang, G.; Xie, Y.; Shen, B.; Gu, Z.; Ding, Y. Delineating the black soil region and typical black soil region of northeastern China. *Chin. Sci. Bull.* **2021**, *66*, 96–106. https://doi.org/10.1360/TB-2020-0178.
34. Ord, J.K.; Getis, A. Local spatial autocorrelation statistics: Distributional issues and an application. *Geogr. Anal.* **1995**, *27*, 286–306. https://doi.org/10.1111/j.1538-4632.1995.tb00912.x.
35. Lv, T.; Zeng, C.; Lin, C.; Liu, W.; Cheng, Y.; Li, Y. Towards an integrated approach for land spatial ecological restoration zoning based on ecosystem health assessment. *Ecol. Indic.* **2023**, *147*, 110016. https://doi.org/10.1016/j.ecolind.2023.110016.
36. Alsafadi, K.; Bi, S.; Abdo, H.G.; Al Sayah, M.J.; Ratonyi, T.; Harsanyi, E.; Mohammed, S. Spatial–temporal dynamic impact of changes in rainfall erosivity and vegetation coverage on soil erosion in the Eastern Mediterranean. *Environ. Sci. Pollut. Res.* **2024**, *31*, 40511–40529. https://doi.org/10.1007/s11356-022-24012-6.
37. Ferreira, C.S.S.; Keesstra, S.; Destouni, G.; Solomun, M.K.; Kalantari, Z. Soil degradation in the Mediterranean region: Drivers and future trends. In *Environmental Sustainability in the Mediterranean Region: Challenges and Solutions*; Ferreira, C.S.S., Destouni, G., Kalantari, Z., Eds.; Springer International Publishing: Cham, Switzerland, 2024; pp. 81–112. https://doi.org/10.1007/978-3-031-64503-7_5.
38. Yang, D.; She, D.; Fang, N.; Huang, X.; Shi, Z. Hydrological connectivity influences soil erosion and SOC loss on vegetation restoration slopes. *Soil Tillage Res.* 2026, *257*, 106991. https://doi.org/10.1016/j.still.2025.106991.
39. Zhang, G.; Xu, T.; Song, J.; Li, Q.; Li, T.; He, B. Characterization of runoff phosphorus loss from a combination of long-term fertilizer application and cultivation on sloping croplands. *J. Hydrol. Reg. Stud.* **2024**, *54*, 101907. https://doi.org/10.1016/j.ejrh.2024.101907.
40. Xu, L.; Li, H.H.; Gao, Y.X.; Dang, W.Q. Impacts of geomorphology and land use/cover change on sediment connectivity in China's Loess Plateau hilly–gully region. *Earth Surf. Process. Landf.* **2026**, *51*, e70375. https://doi.org/10.1002/esp.70375.
41. Chen, H.; Tan, Y.; Xiao, W.; Xu, S.; Meng, F.; He, T.; Li, X.; Wang, K.; Wu, S. Risk assessment and validation of farmland abandonment based on time series change detection. *Environ. Sci. Pollut. Res.* **2023**, *30*, 2685–2702. https://doi.org/10.1007/s11356-022-22361-w.
42. Borrelli, P.; Alewell, C.; Alvarez, P.; Anache, J.A.A.; Baartman, J.; Ballabio, C.; Bezak, N.; Biddoccu, M.; Cerdà, A.; Chalise, D.; et al. Soil erosion modelling: A global review and statistical analysis. *Sci. Total Environ.* **2021**, *780*, 146494. https://doi.org/10.1016/j.scitotenv.2021.146494.
43. Borrelli, P.; Ballabio, C.; Yang, J.E.; Robinson, D.A.; Panagos, P. GloSEM: High-resolution global estimates of present and future soil displacement in croplands by water erosion. *Sci. Data* **2022**, *9*, 406. https://doi.org/10.1038/s41597-022-01489-x.

44. Eekhout, J.P.; de Vente, J. Global impact of climate change on soil erosion and potential for adaptation through soil conservation. *Earth-Sci. Rev.* **2022**, *226*, 103921. https://doi.org/10.1016/j.earscirev.2022.103921.
45. Wu, S.; Chen, L.; Wang, N.; Zhang, J.; Wang, S.; Bagarello, V.; Ferro, V. Variable scale effects on hillslope soil erosion during rainfall-runoff processes. *CATENA* **2021**, *207*, 105606. https://doi.org/10.1016/j.catena.2021.105606.